

Daisy 2D simulation of Rørrendegård

Part of project *Flerdimensional modelling of vandstrømning og stoftransport i de øverste 1-2 m af jorden i systemer med markdræn* for the Danish Environmental Protection Agency.

Søren Hansen <sha@life.ku.dk>
Carsten Petersen <cpe@life.ku.dk>
Per Abrahamsen <abraham@dina.kvl.dk>
Marie Habekost Nielsen <maha@life.ku.dk>
Mikkel Mollerup <mmo@geus.dk>

September 14, 2010

University of Copenhagen
Department of Basic Sciences and Environment
Environmental Chemistry and Physics
Thorvaldsensvej 40
DK-1871 Frederiksberg C
Tel: +45 353 32300
Fax: +45 353 32398

Contents

1	Introduction	3
2	Setup	4
2.1	Weather	4
2.2	Management	4
2.3	Soil profile and biopores	5
2.4	TDR and hydraulic properties	5
2.5	Groundwater table and drain water	6
2.6	Soil bromide and the secondary domain	6
2.7	Particles	9
3	Results	10
3.1	Soil water	10
3.2	Soil bromide	10
3.3	Drains	11
3.3.1	Water	11
3.3.2	Particle leaching	11
3.3.3	Bromide and pesticides	11
4	Discussion	12
4.1	Upper part of the system	12
4.2	Lower part of the system	12
4.3	Bromide and pathways	13
4.4	Further work	13
	References	13
A	Piezometers	16
B	2D plots	22
B.1	Water	22
B.2	Bromide	27
B.3	Pendimethalin	30
B.4	Ioxynil	34
C	Time series	36
C.1	Soil water content	36
C.2	Soil bromide content	36
C.3	Drain content	36

Chapter 1

Introduction

The Rørrendegård site is part of the Copenhagen University experimental station at Tåstrup. It was selected for the present project mainly because of the high resolution flow proportional drain data collected as part of the Agrovand project in the four drain seasons between 1998 and 2002, which included soil particles, a likely transport path for strongly sorbing pesticides. The results of the Agrovand project have been partly documented in Petersen et al. (2001) (biopores), Petersen et al. (2002) (particles and pesticides), Petersen et al. (2004) (particles and bromide), and Petersen et al. (2008) (anisotropy). Furthermore, investigations at the site on tillage effects on soil structure stability and hydraulic properties of the surface layer was reported in Daraghmeh et al. (2008, 2009).

The main focus of the Agrovand project was the influence of tillage on the soil as a transport medium, so four plots with different tillage strategies were followed. In this project we have only studied the data from plot 4, representing conventional tillage, and only the first three seasons, where the best data is available. Apart from particles, the drain water has been analysed for bromide (one application), pendimethalin (two applications) and ioxynil (one application), which we have chosen to include in our simulations. Soil water status has been followed with piezometers, tensiometers, and TDR probes. The most stable results are from the TDR probes, and they are the only one we have used directly for our calibration. The piezometer measurements have been analyzed for use in calibration of the lower boundary, see appendix A. Furthermore, transport pathways have been explored using dye tracer, and biopores have been counted both in the original project, and in more details forming the basis for the new Daisy biopore model in the present project (Nielsen et al., 2010b,a; Nielsen, 2010).

The goal for the simulations presented in this paper is to test two subcomponents of the newly developed 2D Daisy against real data: The first is the particle generation and filtration modules; the second is the slow/fast water movement. For the later, we will use the drain bromide data which are available at a high resolution, and where we have reliable soil measurements to back them up with. The pesticide data is presented together with uncalibrated simulation results as the PLAP sites have more detailed pesticide data available (Lindhardt et al., 2001; Kjær et al., 2009; Hansen et al., 2010a). The Agrovand data is a useful supplement though, as we don't have particle data for the PLAP sites, and the PLAP bromide suffer from the fact that the application was in spring, meaning an unknown amount have been uptaken by the crop. In Agrovand the bromide application was in the autumn, minimizing the potential plant uptake. Instead, the agrovand bromide may have been affected by the formation of ice in the soil, which is not simulated.

Chapter 2

Setup

The Agrovand data has been used from the beginning of the current project for developing the new model, giving the final setup a rich history.

1. An initial setup was developed for water and bromide using the original Daisy model by Tilde Hellsten, as part of her Master Thesis (Hellsten, 2007).
2. A setup for water using the new 2D model was developed by Nanna Gudmand-Høyer, as part of her Master Thesis (Gudmand-Høyer, 2008).
3. This 2D setup was extended for bromide, particles, and pesticides by Mikkel Mollerup, and used as a basis for the PLAP site calibration (Hansen et al., 2010a).
4. Based on the model changes and experience gained made during the PLAP site calibration, the setup was recalibrated by Per Abrahamsen Hansen et al. (2010b).

This history does mean that the setup likely contain parameter choices that no longer are applicable due to changes in the model, and that a new setup made from scratch could be simpler or give better results, had time permitted.

2.1 Weather

All weather data with the exception of precipitation was collected at a station located at Højbakkegård. Three sources were considered for precipitation. Hourly measurements 1.2 meter above ground at the field in the drain seasons, hourly measurements at Højbakkegård also 1.2 meter above ground, and daily measurements at ground level.

As a starting point, we used the hourly field measurements for the drain season, supplemented with the hourly measurements from Højbakkegård for the rest of the season. These were compared with the daily measurements. Where the daily measurements showed precipitation but the hourly measurements didn't we examined the TDR measurements near the surface. If they indicated precipitation, the daily were used to supplement the hourly measurements. Comparison of monthly sums between the hourly and daily precipitation data indicated no systematic bias, thus the hourly data were used without correction for possible effect of wind and snowfall.

Whether the precipitation falls as snow or rain will obviously affect the drain flow, especially at short time scale. Unfortunately, we did not have direct measurements of the type of precipitation. A build-in model of Daisy will let an increasing amount of the precipitation fall as snow when the air temperature drops below 2 °C. This works reasonable well for long time simulations, but not when we as here are interested in the individual events. For simplicity, we chose to fully disable this snow model, so all precipitation in the simulation will fall as rain.

The final weather data is shown on the top graphs of figures C.1 to C.13.

2.2 Management

All seasons had winter wheat with mineral fertilizer, with one plowing operation between harvest and sowing. For Daisy, the dates of the plowing, sowing and harvest is used (table 2.1).

Furthermore, Daisy uses information about the seed bed preparation. As we have not enabled nitrogen in the simulation, the fertilization operations are irrelevant. We use default parameters for the tillage operations. For the harvest, we specify 8 cm stub and that stems and leaves are left on the field. However, since we have not enabled a model for above ground litter, and we are not interested in soil organic matter, that information is not used in the simulation.

In the 2004 and 2005 seasons, the potential evapotranspiration for a winter wheat on the experimental field was measured using an eddy covariance system, and from this a dynamic crop factor was calculated (Kjaersgaard et al., 2008). The the default parametrization was adjusted based on this, and furthermore as part of calibration of soil water the max penetration depth was increased to 1.5 meter, and the interception coefficient were lowered to 0.05 mm per LAI.

Table 2.1: Dates for crop management operations. The initial crop was sowed 1997-9-23.

Operation	1998	1999	2000
Harvest	8-20	8-20	8-20
Plowing	9-15	9-15	9-15
Sow	9-23	9-27	10-18

Date and amount are specified for pesticide and bromide applications. The model setup described in Hansen et al. (2010a) was duplicated here, with field values for DT50 and K_{OC} taken from PPDB (2009). No calibration was done on the pesticides. See table 2.2.

Table 2.2: Pesticide and bromide application.

Date	Name	Amount [g/ha]	DT50 [d]	K _{OC} [ml/g]
1998-11-24	Bromide	34000		
1999-11-16	Pendimethalin	2000	90	15744
2000-11-10	Pendimethalin	2000		
	Ioxynil	200	5	276

All management operations are assumed to be performed at noon.

2.3 Soil profile and biopores

The soil profile and the description of the drain ditch is based on the work presented in Nielsen (2010), where ISSS4 texture classification was used. Petersen et al. (2001) presents texture and dry bulk density (ρ_b) analyses for four depths, which have been used as basis for the main horizons. Unfortunately, no measurements for the C horizon is presented, instead we use the measurement from the bottom of the B horizon (85–90 cm). The Ap measurements (10–15 cm) vary between treatments and between spring and autumn, we have used the spring values for T4 (conventional tillage). The soil humus data are from plot A in Petersen et al. (2002). The values used are summarized in table 2.3.

Initially, three classes of biopores were used in the simulation based on Nielsen et al. (2010b), where we focused on the biopores that potentially had connection to the drain pipes. We first assumed that all the deep biopores (the two classes ending in 120 cm) in the drain ditch would be directly connected to the drain pipes. Based on pesticide measurements in drains in the PLAP sites, we decided to change this so only half the deep biopores in the drain ditch would be directly connected to the drain pipes (Hansen et al., 2010a). Compared to the PLAP simulations, we had additional soil bromide measurements (section 2.6), so we decided to add an extra class ending halfway down. The measurements of Petersen et al. (2001) indicated a roughly linear decrease of biopore density with depth, so we chose to use the same density as for the full length biopores. The classes are summarized in table 2.4.

The organic matter and nitrogen modules were disabled.

2.4 TDR and hydraulic properties

HYPRES was used initially to estimate hydraulic properties for all horizons. The TDR measurements (see figure C.1) have been used for calibrating. The only parameter that has been changed

Table 2.3: Soil properties. Depth is specified in cm below soil surface, and the dry bulk density (ρ_b) specified in g/cm^3 . Humus is given as a percentage of total weight. For the drain ditch, where the ISSS4 texture classification system was used, the mineral soil particle distribution is also given as fraction of total weight. For the other horizons the USDA3 system was used, and the mineral soil particle distribution is given as percentage of total mineral weight.

Horizon	Depth	Clay < 2 μm	Silt < 50 μm	Sand < 2 mm	Humus	ρ_b
Ap	0–25	10.7	22.2	67.1	3.0	1.49
Plow pan	25–33	14.8	21.4	63.8	1.6	1.70
Bt	33–120	22.2	19.5	58.3	1.6	1.65
C	120–200	20.7	23.5	55.8	1.0	1.69

Area	Depth	Clay < 2 μm	Silt < 20 μm	Fine Sand < 200 μm	Coarse sand < 2 mm	Humus	ρ_b
Drain ditch	33–120	21.3	19.0	24.4	33.9	1.4	1.65

Table 2.4: Biopore classes.

Depth	cm	0–25	0–120	30–120	0–60
Diameter	mm	2	4	4	4
Density	m^{-2}	100	23	7	23

is K_{sat} (saturated conductivity). For the surface layer (top 3 cm), this has been decreased to 10% of the value suggested by HYPRES. In the Bt horizon conductivity has been decreased to 50%, and in the C horizon it has been tripled. The result is shown on figure 2.1.

Based on Petersen et al. (2008) we chose to add an anisotropy of 12 (meaning horizontal flow is 12 times faster than vertical) to the plow pan.

2.5 Groundwater table and drain water

An EM38 map of the field indicated large areas to have a sandy underground (Gudmand-Høyer, 2008), and the piezometers showed that these areas had a significantly lower groundwater level (see appendix A). We estimated that roughly two thirds of the field did not contribute to the drainage through the groundwater level. In Daisy we modelled this by dividing the field into two columns. The first column had a free drainage lower boundary, and represented twice the area of the other column, with an aquitard bottom. The aquitard layer was described with a size (2 meters), a conductivity (0.5 mm/h) and the pressure table of the underlying aquifer. The pressure table was based on a median piezometer value (see appendix A), and calibrated to match drain flow, and is shown on figure 2.2. Note that piezometer measurements represent pressure 2.3 m below surface, while the aquifer represents pressure 4 m below surface. The free drainage column would still contribute to the drain water through directly connected biopores. The TDR measurements were performed in the part of the field with clay underground, and the comparisons are therefore done to the column with an aquitard.

2.6 Soil bromide and the secondary domain

We have not included cracks in the description of the conductivity curve, but we still divide water into two domains for the sake of solute transport. This division was calibrated based on bromide soil measurements shown on the top graph on figure C.5. The simulated dynamics shown on figure C.4 were used as a help. The two figures are explained in section 3.2.

The division between water into two domains (the primary “slow” domain and the secondary “fast” domain) is controlled by single horizon specific parameter, h_{lim} , a pressure head. If the actual pressure head (h_a) is below h_{lim} , all matrix water will be part of the primary domain. Otherwise, the water in the soil corresponding to h_{lim} is considered part of the primary domain, and any additional matrix water is considered part of the secondary domain. The water flux calculated by Richard’s equation (q) will be divided so that the primary domain water flux (q_1)

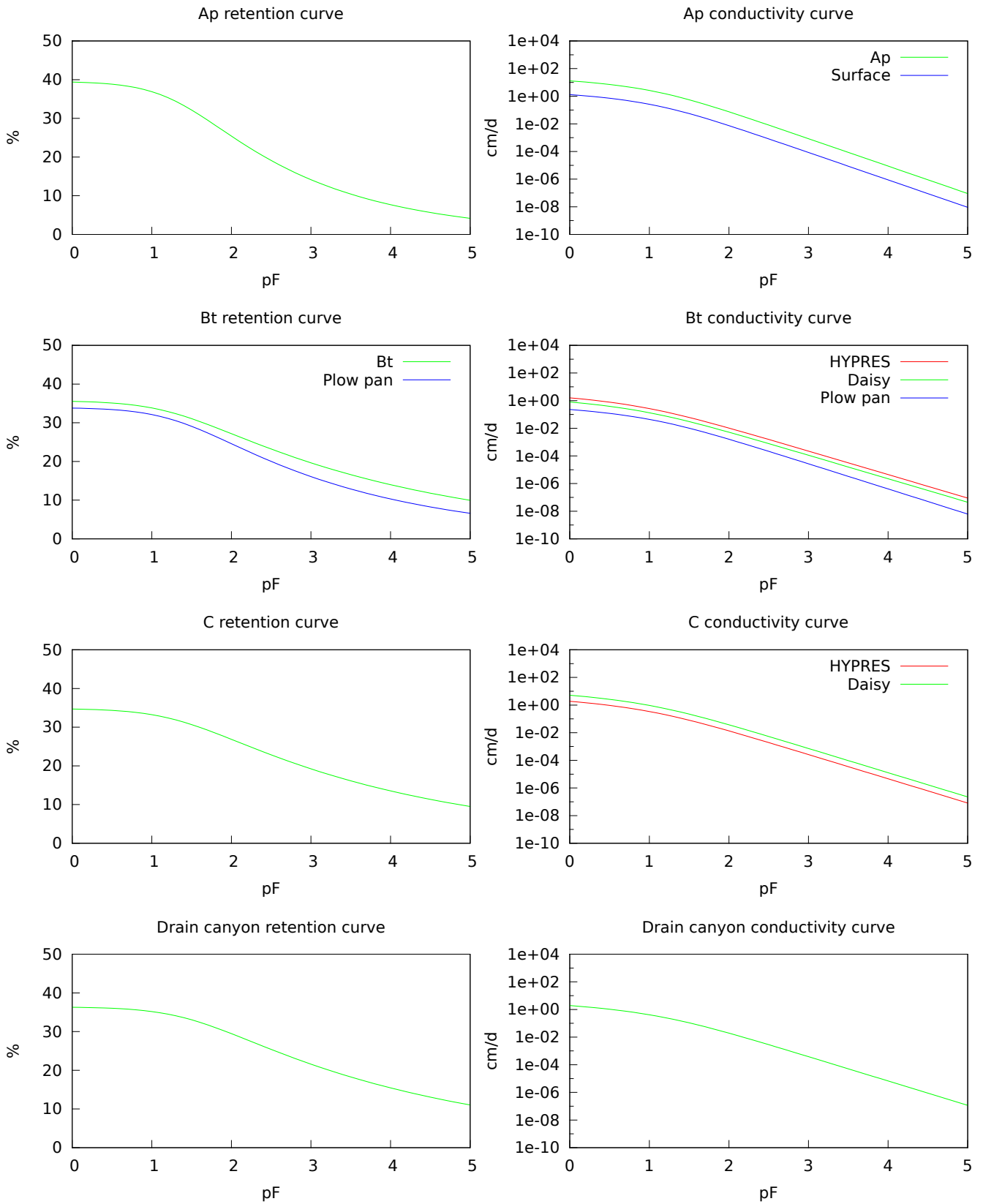


Figure 2.1: Rørrende soil hydraulic properties. HYPRES refers to parameters estimated according to Wösten et al. (1999), Daisy to the final parametrization (ignoring anisotropy and biopores), and surface and plow pan to the conditions at the top of the A and Bt horizons.

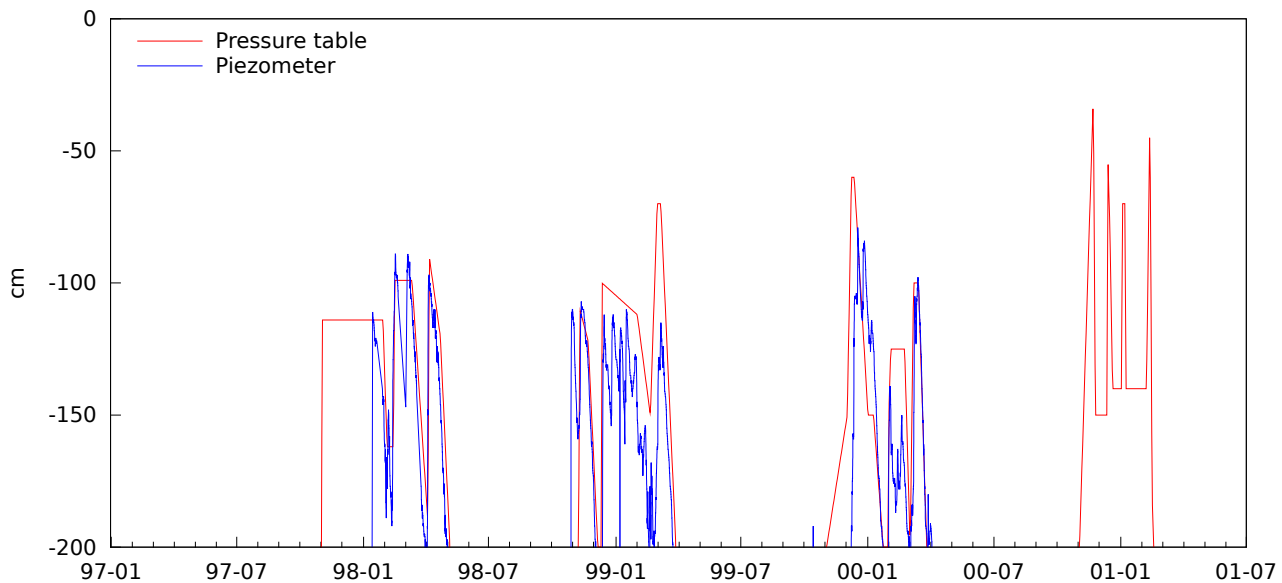


Figure 2.2: Median measured pressure level at 230 cm below surface together with calibrated aquifer pressure level

is

$$q_1 = \frac{K(h_{\text{lim}})}{K(h_a)}$$

where $K(h)$ is the hydraulic conductivity at pressure head h , and the secondary domain water flux (q_2) is $q_2 = q - q_1$. Solute transport in the primary domain is calculated with the convection-dispersion equation, while solute movement in the secondary domain is handled as pure convection. A second parameter, α determines the speed of exchange between the two domains.

The bromide was measured in 25 cm intervals, starting from the soil surface. The measurements show the highest bromide concentrations below 50 cm. The results were based on 16 random samples of each plot, and the pattern were similar in the three other plots. (Petersen et al., 2004). Using a plain one domain convection-dispersion equation, our simulations showed that most bromide should still be in the top 50 cm. In other word, this was a classic case where the convection-dispersion equation, which assumes full equilibrium between solute content in different pore classes, was inadequate. The idea was that by dividing the pore classes in two domains, and calculating transport separately for each domain, the bromide could stay in the secondary domain and move down faster.

As an initial guess, we used $h_{\text{lim}} = 2$ pF and $\alpha = 0.01 \text{ h}^{-1}$, the later taken from Jaynes et al. (1995). Using these values, our initial results were far worse than with the pure convection-dispersion equation. In these simulations, the bromide would stay in the top 25 cm. There were two problems: The soil surface was dry enough that much of solute would enter the primary domain, and stay relatively protected there. Lowering h_{lim} to 3 pF in the soil surface would ensure that all the water (and solute) would enter the secondary domain. The second problem was the long period, over a month, before two large events caused significant leakage out of the plow layer. With an α of 0.01 h^{-1} a month was plenty of time to reach equilibrium, again causing some of the bromide to be protected in the primary domain. We got the best results by lowering α to 0.00003 h^{-1} in the top soil (to the bottom of the plow pan), decreasing it further had little effect.

As the biopores were the main transport mechanism through the plow pan, we added a new biopore class that ended 60 cm below ground, in order not to bypass the 50–100 cm area entirely, see section 2.3. This gave a problem for estimation of α below 33 cm. A too high value would cause some bromide to stick just below the plow pan, where it would count as part of the 25–50 cm interval. A too low value would cause the bromide that were transported down to 60 cm through the biopores to move too fast below 100 cm. We never found a good value. The values

used are listed in table 2.5.

Table 2.5: Two domain solute transport parameters.

Depth [cm]	h_{lim} [pF]	α [h ⁻¹]
0-33	3.0	0.00003
33-	2.0	0.0001

2.7 Particles

Particles in Daisy are generated on the soil surface as a result of rainfall, and then transported down through the soil matrix or biopores. We use the filter function from Jarvis et al. (1999) for the matrix domain. As the matrix domain in Daisy is divided into a primary and secondary domain, we use different filter coefficients for the two domains. We choose values of 80 and 40 m⁻¹ for the primary and secondary domain respectively, in order to stay near the 50 m⁻¹ used in Jarvis et al. (1999). Daisy will (unlike MACRO) not filter particles in the biopores, only in the matrix.

For the particle generation we tried multiple models (Styczen and Høeg-Schmidt, 1988; Morgan et al., 1998; Jarvis et al., 1999), but only Jarvis et al. (1999) gave anything near the desired dynamics. It was also the only of the models designed to match drain measurements, and the only model with a pool of readily available particles. We use the values from Jarvis et al. (1999) as a starting point, except for the maximum particle storage (M_{max}) which is estimated based on the clay content as described in Brubaker et al. (1992), method 1. From calibration, we would initially conclude that the detachment rate coefficient (k_d) should be decreased to 7.5 g/J, the replenishment rate (k_r) to 0.1 g/m²/h, and the depth of the soil affected by detachment and dispersion (z_i) to 0.5 mm. These values were used for PLAP simulations. Later we found that reverting to the values from Jarvis et al. (1999) gave better results, and those values are used for the present simulations.

The results are discussed in section 3.3.

Chapter 3

Results

The main simulation results are presented together with measured data on figures C.1 to C.13, found at the end of the report (appendix C). Additional 2D plots with simulation results without matching measurements can be found in appendix B.

3.1 Soil water

Figure C.1 shows horizontal TDR measurements for different depths. The two autumn gaps are after plowing, when the TDR probes are removed. At the third season the TDR probes had drifted, and were left out. The TDR probes measurements do not include water in the form of ice, which explain the apparent noise in the measurements during periods with frost. Enabling the experimental support for ice in Daisy showed a good match between upper TDR probes and simulated water during the two winter periods, supporting the idea that difference is due to ice (see figure C.2). Unfortunately, the ice support in Daisy is not yet complete, and enabling it created too many other problems with the simulation, so it was disabled for the final runs. The simulation overestimates the water level near the soil surface, which could possibly be a problem with the TDR measuring some air. We may overestimate the dynamics near the bottom of the plow layer. The measurements for the bottom TDR show fast variations during the winter which looks mostly like noise, something not duplicated in the simulation, with or without ice.

Figure C.3 shows the same data for the first summer after installation. The general water level seems to be slightly overestimated at the end of the period, except in the 60 cm TDR where it is underestimated.

3.2 Soil bromide

The measured and simulated bromide content in the top four 25 cm intervals is shown on the second graph in figure C.5. The period is from right before application, to right after the soil measurement.

As can be seen, the content of 00-50 cm is slightly overestimated in the simulation, while the content of 50-100 cm is underestimated. The two next graphs below that divide the content in the same intervals into the primary domain (small pores, slow water movement) and the secondary domain (large pores, fast water movement). The remaining graphs shows bromide transport through the borders between the soil intervals. As can be seen, the bromide enter the soil through the secondary domain, and some move further down through the secondary domain at 25 cm, but most bromide are moved down through the tertiary domain (the biopores), There is no significant transport in the primary domain. However, at the end of the period the primary domain dominate storage.

In figure C.7 we examine four additional intervals the same way, namely 25-33 cm (plow pan), 33-50 cm, 100-125 cm (end of long biopores), and 125-150 cm (below biopores). As can be seen, the first events bring down bromide with both the medium depth biopores that end in the 50-75 cm interval, and the deep biopores that end in the 100-125 cm interval. But the later events apparently mostly activate the deep biopores.

Figure C.4 shows the usual weather graph at the top. Next is a graph showing how the water enter the system. We see that the first rain after application enter the soil through the secondary domain. So does most of the remaining rain, but some events result in ponding above the threshold for activating surface biopores, as shown on the third graph. The bottom five graph correspond to the bottom five graphs of figure C.5, except the values are not accumulated. Figure C.6 is similar, except that the four bottom graphs represent the additional intervals from figure C.7.

3.3 Drains

The full drain seasons are depicted on figure C.8, C.10, and C.12, while figure C.9, C.11, and C.13 focus on a single event within each drain season.

3.3.1 Water

The top graph of all figures show precipitation and temperature for the period. The next graph shows simulated and observed drain flow, as well as calibrated aquifer and measured median piezometer pressure. Below that we get accumulated drain flow, simulated and observed. By calibrating the aquifer pressure (see figure A.5), we were able to match total drain flow, however we consistently underestimate the dynamics of each event. Furthermore, in the beginning of the first season we get too much water, despite using a very low aquifer pressure compared to the piezometer data, and for the second season we have the opposite problem.

3.3.2 Particle leaching

The next two graphs concern particle leaching. In the first we see flow proportional particle leaching, with simulated values extracted the same time as measurements. Each data point represents the accumulated value since last measurement. We also plot the simulated reservoir of readily available particles from the Jarvis et al. (1999) model. The next graph show accumulated values, as well as simulated water flow directly from surface to drain. In general we see that the measurements tend to be taken when Daisy predict the deep biopores to be active (that is, when there is heavy rain). The dynamic simulation rarely match measurements, but the accumulated numbers show that seen over an event the simulation is more often a good match. Not always though, which means Daisy overestimate total particle leaching the first year, and underestimate it the last year. In general, the variation in the measured numbers is larger than the variation in the simulated numbers.

3.3.3 Bromide and pesticides

The next graphs vary by season. Simulated and observed concentration of bromide and pesticides are shown for the seasons where they were measured. For bromide, we also show accumulated values. For pesticides, where there are far fewer measurements, we instead show dynamic leaching.

The bromide simulation has too high concentration at the beginning of the season, especially during the first large event that activates the biopores. The simulated bromide concentration is too low at the end of the season. The second season continue this trend, with too low concentrations.

For both pesticides, the general trend is that we simulate too high concentrations in the drain water. However, since we often underestimate the water flow during the events, the total simulated drain leaching is closer to what is measured. We can also see that the strongly sorbing pendimethalin are almost exclusively leach together with particles, while ioxynil is found both particle bound and dissolved.

Chapter 4

Discussion

The simulation results can roughly be divided into three categories. The first category is the results that depend mostly on the upper part of the system. These include TDR probes, drain particles, and pesticide leaching through drains. The second category is the results that depend mostly on the lower part of the system. These include piezometers and drain water measurements. The final category is the bromide measurements in soil and drains.

4.1 Upper part of the system

The fine dynamic match between the TDR probes and simulation results gives us faith in both our upper boundary, and in our description of the part of the soil monitored by the probes. The only caveat here is the effect of ice and snow, which was not included in our final simulation.

During calibration, we found that the amount of particles simulated in drain pipes was robust with regard to changes to the lower boundary, so we include those results with the upper part of the system. Getting the right level of particles seen over three seasons using the parameters from Jarvis et al. (1999), only adjusted for clay content as specified in Brubaker et al. (1992), is encouraging. We would have liked to see the same variation between seasons as we measured though, and the timing within events could be better.

The *mass* of simulated pesticide leaching through the drain pipes is also relatively robust with regard to changes in the lower boundary as well. The *concentration* is not, though, as changes in the lower boundary will greatly affect the amount of water in the drain pipes. The explanation is that the simulation has half (ioxynil) or nearly all (pendimethalin) the amount leached being particle bound. This obviously makes the particle model crucial, and also the *soil enrichment factor* pesticide parameter, which specifies how more likely the pesticide is to bind to a particle. That particular parameter were given an initial value of 10000 in order to see an effect, and has not been calibrated afterwards. The sorption kinetic is similarly not based on literature values, nor calibrated. A (de)sorption rate of 0.05 h^{-1} was chosen too see an effect given the Daisy timestep of hour. With these caveats taken into account, the results are encouraging.

4.2 Lower part of the system

There are several warning signs for the lower boundary of the systems. First, less than 5% of the yearly precipitation finds its way to the drain pipes, meaning small variations in the total system can lead to large variations in the drain pipes. Related to this, the EM38 map suggest that large parts of the field has a sandy underground, and are unlikely to contribute to the drain flow. Finally, the piezometers show great spatial and temporal variation, and indicate that different parts of the field may contribute to the drain flow at different times. As we sometimes have significant drain flow when the piezometers show low pressure, this could indicate that local areas of shallow groundwater may be at play. The rightmost graph on the second row on figure B.1 could be an example of this.

Dividing the field into two parts, one with free drainage and one with an aquitard bottom, is not enough to catch this spatial variation. The main problem is our inability to catch the dynamic effect in the drain that occurs a few hours into a large event. Figure A.5 shows the other

side of this, our simulated groundwater table is much more stable than the median piezometer measurements, despite the later representing pressure 2.3 m below ground level.

4.3 Bromide and pathways

The soil measurements show that largest amounts of bromide should be located between 50 and 100 cm below soil surface at the end of the first drain season. Of the 34 kg/ha applied, 15 were found at that interval, 7 above, and the remaining 12 were lost. The same general pattern were found on the three other plots. This fits well with the drain measurements, that shows the largest leaching (with the highest concentrations) occurring near the end of the drain season.

We were unable to duplicate this in the simulation. Traditional convection-dispersion would not move the bromide far enough down. Distinguishing between transport with slow and fast water tended to worsen the results, as the bromide stayed long enough in the top soil after application to move into the primary domain (slow water), where it would be protected. An uncertainty of the system was when the bromide would enter the soil, as the surface was frozen at the time of application. Delaying the entrance to the soil in the simulation to right before the first large event would prevent the bromide from entering the primary domain, but not leave enough time for it to move below 50 cm.

Adding an additional class of biopores that ended at 60 cm did help. The effect can be seen on the top left graph of figure B.5. However, as the top right graph shows, the main part of the bromide later move down to end of the long biopores. The same effect can be seen on figure C.4 and C.5. The first event activate both biopore classes, the later events mostly the deep biopores.

In general, this indicates a problem with our model of the pathways in the system, which will likely have some affect not only bromide but also on particles and pesticides.

4.4 Further work

There are still more work to be done on calibration of the current version of the model for the agrovand dataset. The problems with the lower boundary is probably more than we can solve, but the bromide pathways is a problem that should be solvable with the present model.

The agrovand dataset can also provide basis for further model development. Ice obviously had an influence on the TDR measurements (see figure C.2, especially the first season. This could be used for finishing the ice module of Daisy, and would increase the trustworthiness of the simulation for that season, especially when coupled with the drain measurements. The effect of frost on particle generation, as examined by e.g. Kværnø and Øygarden (2006) would be relevant. And of course, ice may also affect the water pathways, and possibly cast light on the bromide results.

The largest potential in the dataset resides in the three other plots with different tillage regimes. This dataset could be used for developing a model that included the effect of tillage on soil surface properties and particle leaching, and consequently on leaching of strongly sorbing pesticides. A better model that would include tillage more directly might help explain the difference we measured between the three seasons.

Preliminary results from the project *Undersøgelse af makroporekontinuitet ved markdræn og effekter af direkte forbundne makroporer på jords filterfunktion* indicate that the zone around the drain pipes is wider than assumed in this project, which would help explain some of the observed drain water dynamics. Thus, adjusting the setup to take these results into account would be an interesting avenue of investigation.

Finally, we need better estimates for (de)sorption rates and the soil enrichment factor, either from literature or from focused experiment.

Bibliography

- Brubaker, S. C., Holzhey, C. S., and Brasher, B. R. (1992). Estimating the water-dispersible clay content of soils. *Soil Science Society of America Journal*, 56(4):1226–1232.
- Daraghmeh, O., Jensen, J., and Petersen, C. (2008). Near-Saturated Hydraulic Properties in the Surface Layer of a Sandy Loam Soil under Conventional and Reduced Tillage. *Soil Science Society of America Journal*, 72(6):1728–1737.
- Daraghmeh, O., Jensen, J., and Petersen, C. (2009). Soil structure stability under conventional and reduced tillage in a sandy loam. *Geoderma*, 150(1-2):64–71.
- Gudmand-Høyer, N. (2008). 2d-modelering af vandtransport i jord. Master’s thesis, University of Copenhagen.
- Hansen, S., Abrahamsen, P., and Pederen, C. (2010a). Daisy 2D simulation of Silstrup and Estrup. Technical report, University of Copenhagen.
- Hansen, S., Pederen, C., Abrahamsen, P., Nielsen, M. H., and Mollerup, M. (2010b). Daisy 2D simulation of Rørrendegård. Technical report, University of Copenhagen.
- Hellsten, T. (2007). Vand- og stoftransport til grundvand og markdræn belyst ved udvaskningsforsøg og daisy-modellering. Master’s thesis, University of Copenhagen.
- Jarvis, N. J., Villholth, K. G., and Ulén, B. (1999). Modelling particle mobilization and leaching in macroporous soil. *European Journal of Soil Science*, (50):621–632.
- Jaynes, D., Logsdon, S., and Horton, R. (1995). Field method for measuring mobile/immobile water content and solute transfer rate coefficient. *Soil Science Society of America Journal*, 59(2):352–356.
- Kjær, J., Rosenbom, A. E., Olsen, P., Ernstsen, V., Plauborg, F., Grant, R., Nyegaard, P., Gudmundsson, L., and Brüsch, W. (2009). The Danish pesticide leaching assessment programme: Monitoring results may 1999 – june 2008. Technical report, GEUS.
- Kjaersgaard, J., Plauborg, F., Mollerup, M., Petersen, C., and Hansen, S. (2008). Crop coefficients for winter wheat in a sub-humid climate regime. *Agricultural Water Management*, 95(8):918–924.
- Kværnø, S. and Øygarden, L. (2006). The influence of freeze-thaw cycles and soil moisture on aggregate stability of three soils in Norway. *Catena*, 67(3):175–182.
- Lindhardt, B., Abildtrup, C., Vosgerau, H., Olsen, P., , Torp, S., Iversen, B. V., Jørgensen, J. O., Plauborg, F., Rasmussen, P., and Gravesen, P. (2001). The Danish pesticide leaching assessment programme: Site characterization and monitoring design. Technical report, GEUS.
- Morgan, R., Quinton, J., Smith, R., Govers, G., Poesen, J., Auerswald, K., Chisci, G., Torri, D., and Styczen, M. (1998). *EUROSEM: Documentation and user guide*. Cranfield University, 3.6 edition. The European Soil Erosion Model.
- Nielsen, M. H. (2010). *On preferential flow pathways in and between drain trenches in a sandy loam — a study of quantity, distribution and connectivity of macropores and the distribution of Brilliant Blue, bromide and 1 µm microspheres along macropores*. PhD thesis, University of Copenhagen.

- Nielsen, M. H., Styczen, M., Ernstsens, V., Petersen, C. T., and Hansen, S. (2010a). Distribution of bromide and microspheres along macropores in and between drain trenches. *Vadose zone J.* accepted.
- Nielsen, M. H., Styczen, M., Ernstsens, V., Petersen, C. T., and Hansen, S. (2010b). Field study of preferential flow pathways in and between drain trenches. *Vadose zone J.* accepted.
- Petersen, C., Hansen, S., Jensen, H., Holm, J., and Koch, C. (2004). Movement of suspended matter and a bromide tracer to field drains in tilled and untilled soil. *Soil Use and Management*, 20(3):271–280.
- Petersen, C., Holm, J., Koch, C., Jensen, H., and Hansen, S. (2002). Movement of pendimethalin, ioxynil and soil particles to field drainage tiles. *Pest management science*, 59(1):85–96.
- Petersen, C., Trautner, A., and Hansen, S. (2008). Spatio-temporal variation of anisotropy of saturated hydraulic conductivity in a tilled sandy loam soil. *Soil and Tillage Research*, 100(1-2):108–113.
- Petersen, C. T., Jensen, H. E., Hansen, S., and Koch, C. B. (2001). Susceptibility of a sandy loam soil to preferential flow as affected by tillage. *Soil and Tillage Research*, 58(1-2):81 – 89.
- Styczen, M. and Høeg-Schmidt, K. (1988). A new description of splash erosion in relation to raindrop sizes and vegetation. In Morgan, R. and Rickson, J., editors, *Erosion assessment and modelling*. Commission of the European Communities, EUR 10860.
- PPDB (2009). The Pesticide Properties Database (PPDB). Developed by the Agriculture & Environment Research Unit (AERU), University of Hertfordshire, funded by UK national sources and the EU-funded FOOTPRINT project (FP6-SSP-022704).
- Wösten, J., Lilly, A., Nemes, A., and Bas, C. L. (1999). Development and use of a database of hydraulic properties of European soils. *Geoderma*, 90:169–185.

Appendix A

Piezometers

A total of 63 piezometers were installed 2.3 m below soil surface for all four plots, 70 cm, 4 m and 8 m from each side of the drain pipes, and 10, 40, and 70 m from the sampling wells.

Individual measurements from plot 4 for the two seasons are shown on figure A.1 and A.2. To impose some order, we chose to look at the median values, as shown on figure A.3 and A.4. The top graphs shows that there generally is higher pressure further away from the drain pipes, at least in the periods where the pressure is high and the drains are likely to be active. When the drains are inactive, there is no clear trend. The middle graphs show highest pressure closest to the well, and that at a distance of 70 m, the pressure is rarely high enough to indicate drain activity. The only clear trend shown in the bottom graph is that the pressure at plot 1 is lower than the pressure at the remaining three plots.

In order to have a single piezometer value for use in calibration of the lower boundary of the system, we want as many piezometer measurements as possible, to weed out local variations. But we only want piezometer measurements from those part of the field that contribute to the drain flow. A EM38 map of the field indicate that the underground is more dominated by sand around 50 m from the wells, and that plot 1 likely contain more sand than the other three (Gudmand-Høyer, 2008). As this matches well with our analysis of the piezometer measurements, we choose to include plot 2, 3 and 4 at 10 m and 40 m distance from the wells, in our final median piezometer value, shown on figure A.5 together with our calibrated aquifer pressure, and simulated groundwater table.

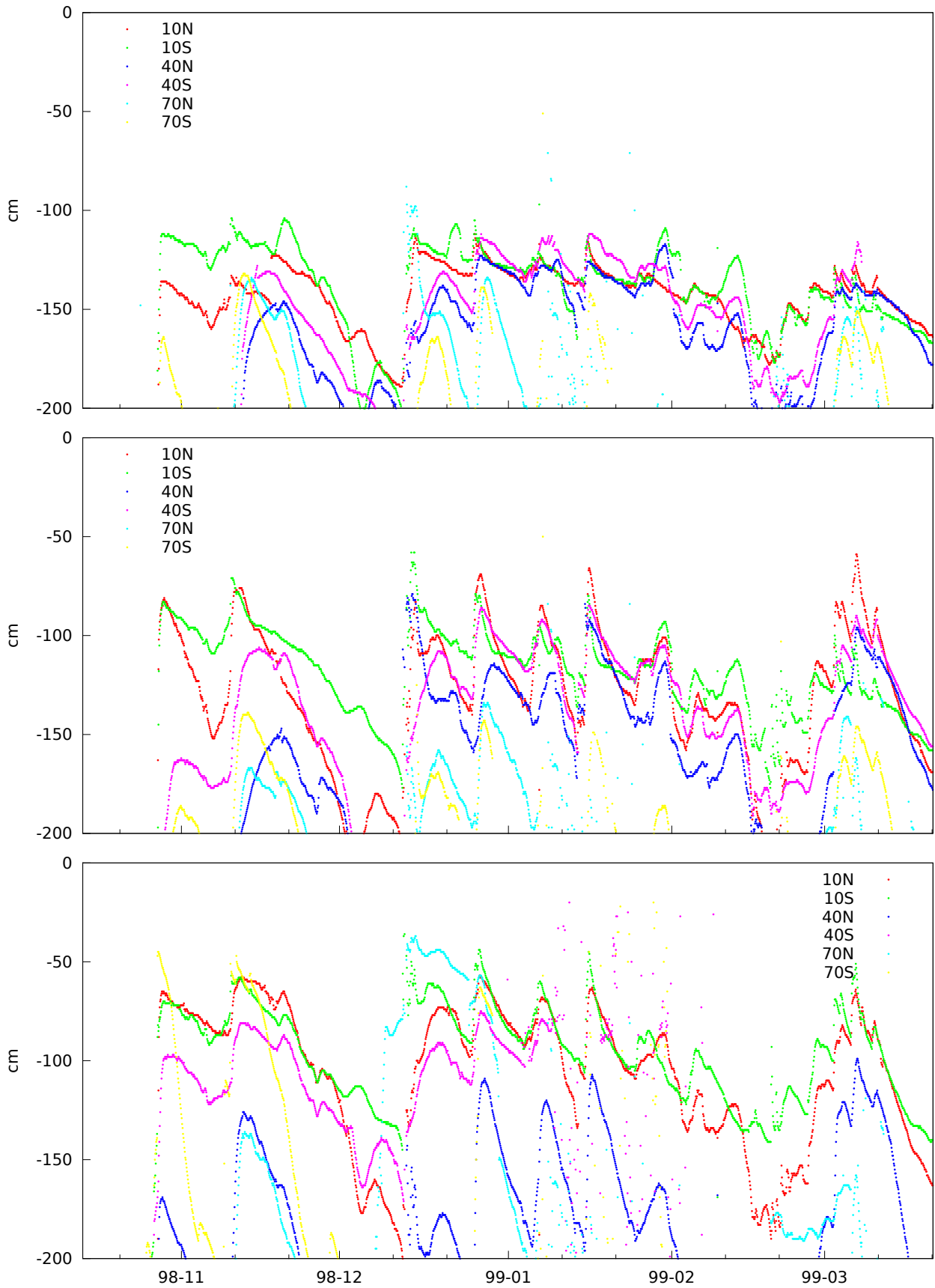


Figure A.1: Pressure at 230 cm below surface, 70 cm (top), 4 m (middle) and 8 m (bottom) from drain. First drain season, plot 4. The labels indicate distance from drain well (in meters) and whether the piezometer is located North or South of the drain pipe.

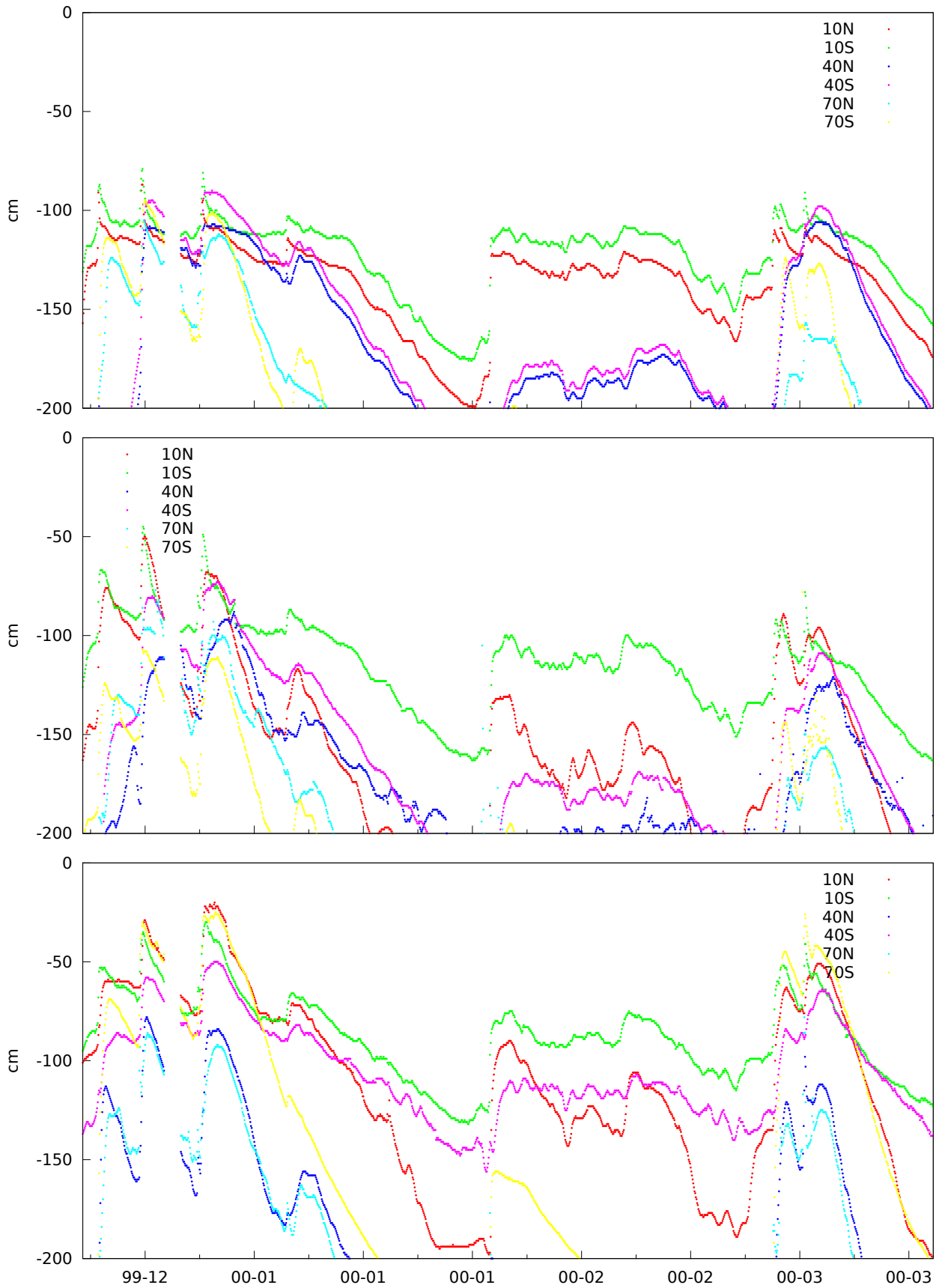


Figure A.2: Pressure at 230 cm below surface, 70 cm (top), 4 m (middle) and 8 m (bottom) from drain. Second drain season, plot 4. The labels indicate distance from drain well (in meters) and whether the piezometer is located North or South of the drain pipe.

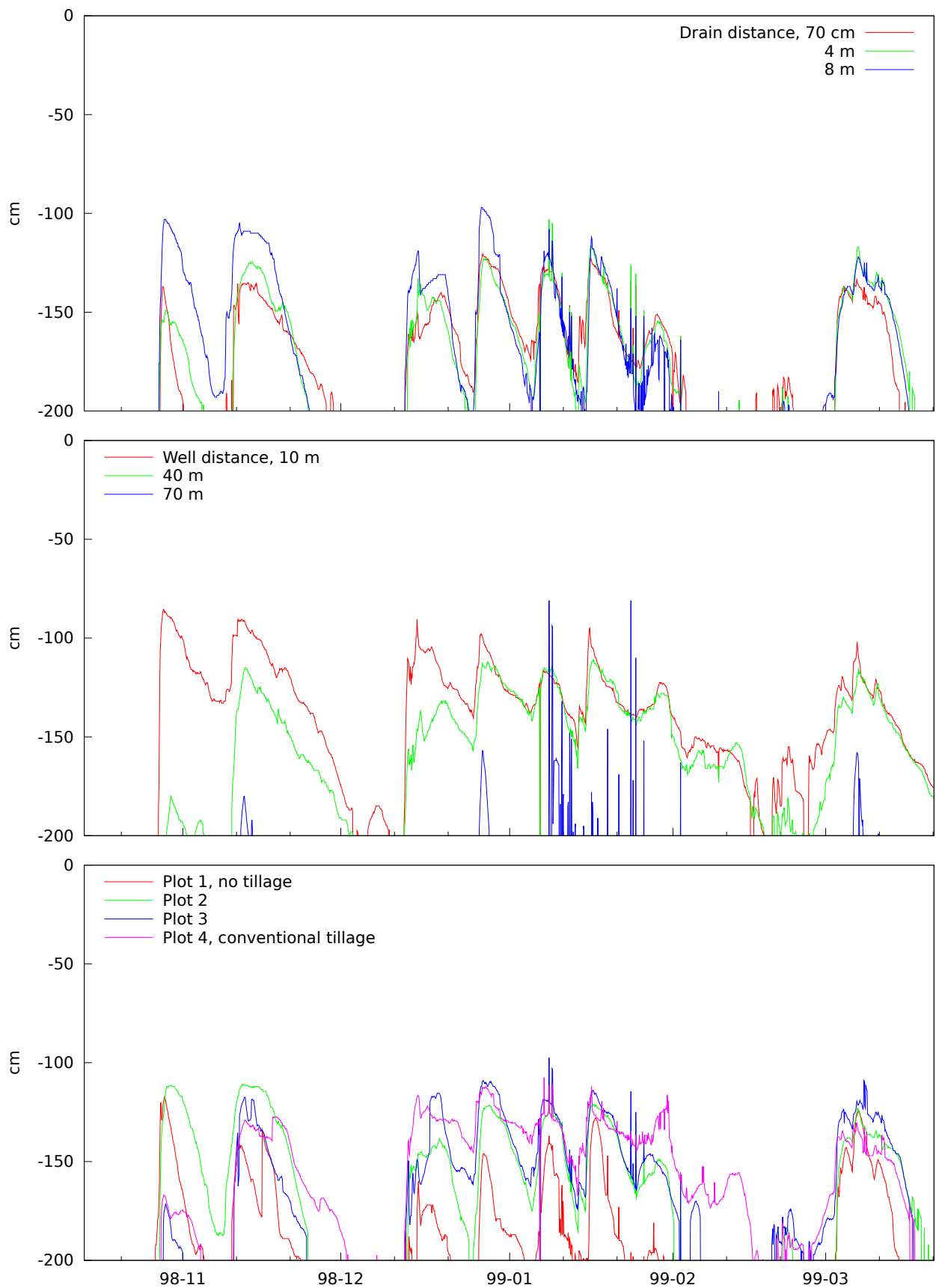


Figure A.3: Median measured pressure level at 230 cm below surface for first drain season. Top graph show distance from drain, middle graph distance from well, and bottom graph plot number.

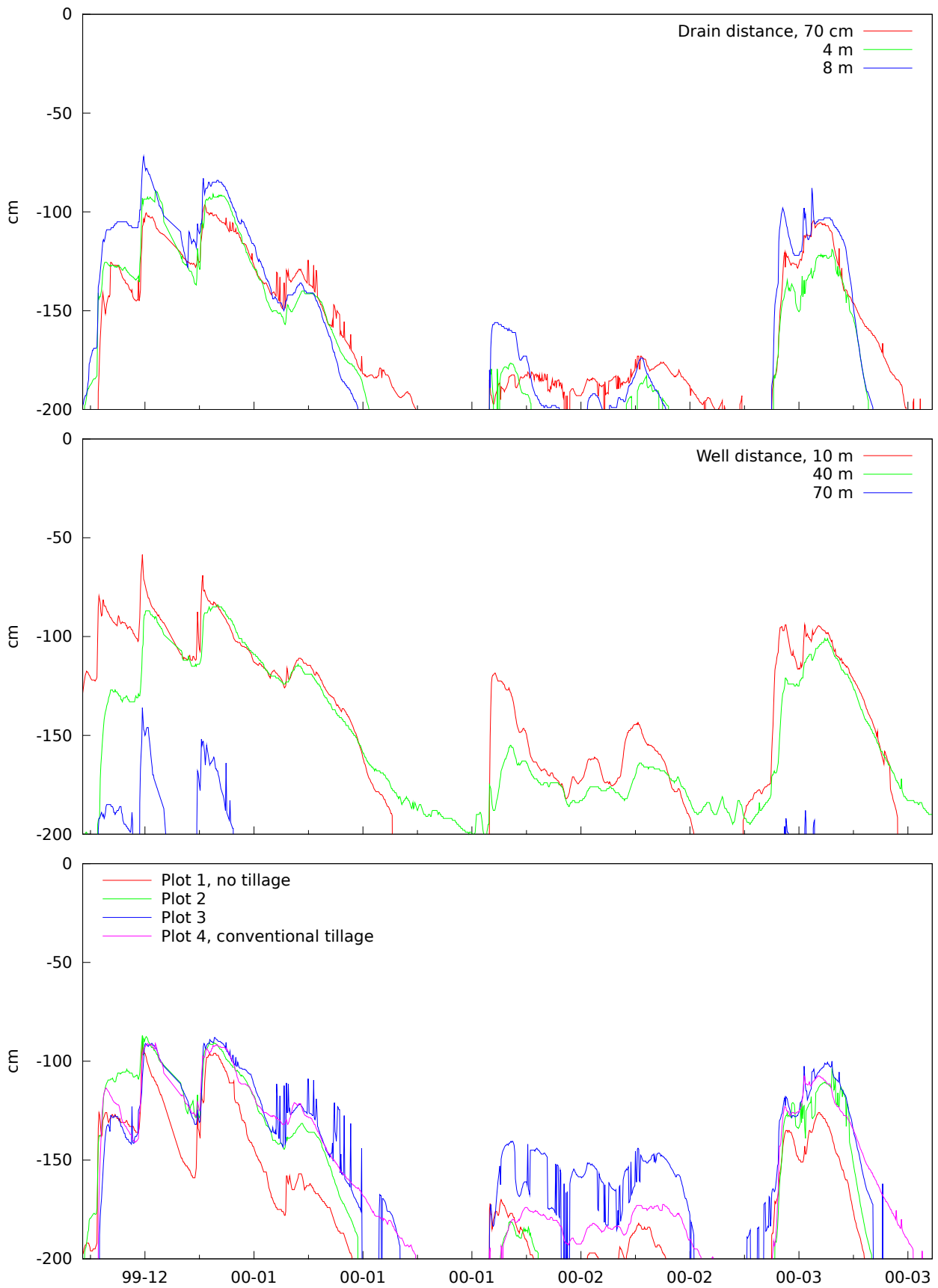


Figure A.4: Median measured pressure level at 230 cm below surface for first drain season. Top graph show distance from drain, middle graph distance from well, and bottom graph plot number.

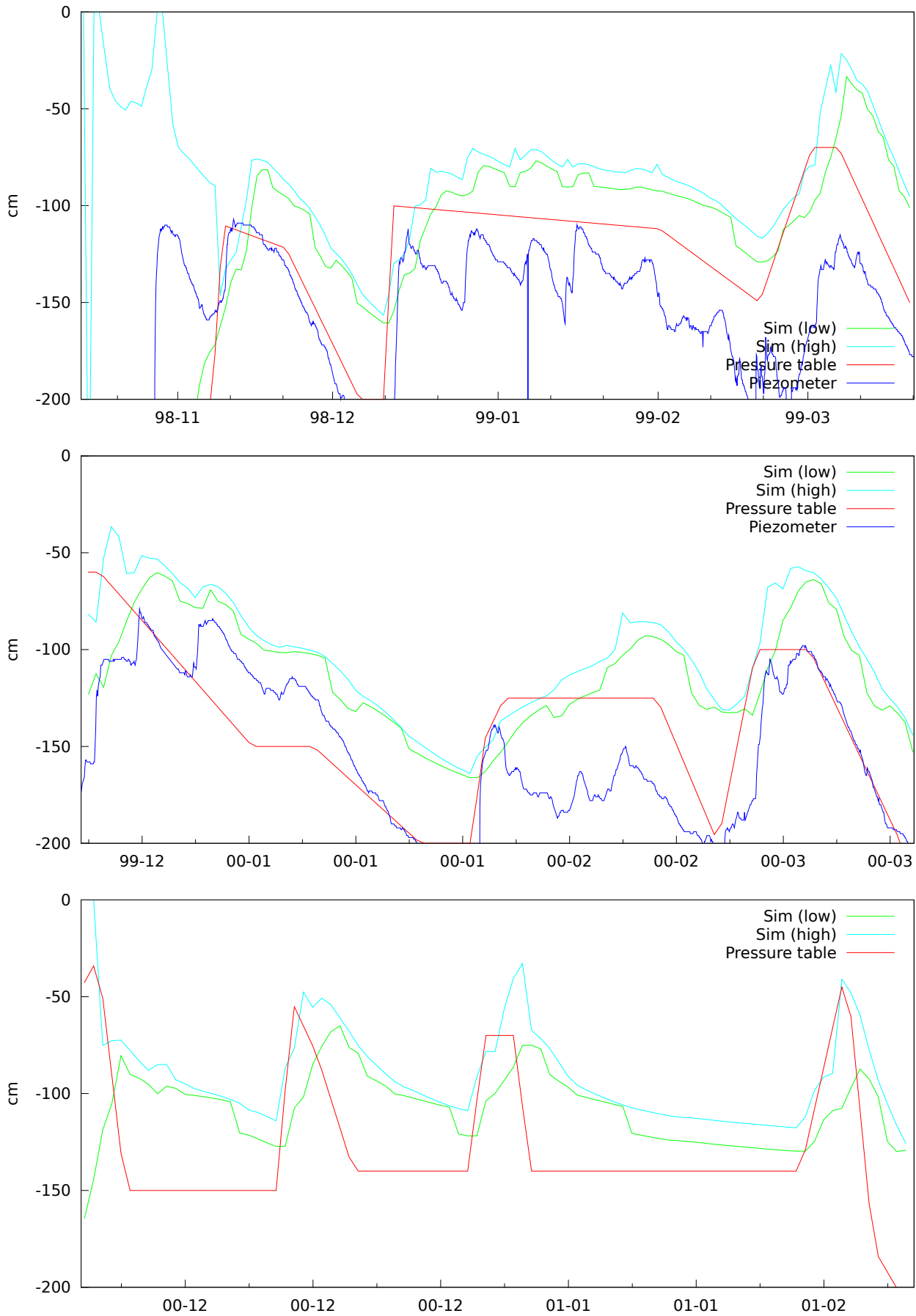


Figure A.5: Median measured pressure level at 230 cm below surface together with calibrated aquifer pressure level and simulated groundwater table. Simulated low value is calculated from pressure in lowest unsaturated numeric cell, typically located near drain. Simulated high value is calculated from pressure in highest saturated cell, typically farthest away from the drain. The sudden jumps of the high value represents situations with surface ponding, where the top numeric cell becomes saturated.

Appendix B

2D plots

In this appendix we present simulated 2D plots for water, bromide, pendimethalin, and ioxynil. The simulated values presented here are all from the part of the soil with an aquitard bottom. There are no measurements to compare with, a major caveat for both the results and discussion. We use two kinds of graphs to capture the 2D structure.

The first kind depict static distribution in the soil. Each graph has horizontal distance from drain on the x-axis and height above surface on the y-axis, using the same scale for both axes. The graph represents the the computational soil area used in the simulation. The right side is the center between two drains (8 meter for Rørrende), and the bottom is 2 meter below ground, where we use an aquitard lower boundary with a calibrated aquifer. The graphs are color coded, where specific colors represent specific values for the soil. Each numeric cell in the computation has a color representing the value within that cell. Since cells are rectangular, the graphs appear blocky.

The second kind of graph depicts horizontal or vertical movement. For the graphs depicting horizontal movement, the y-axis specifies height above surface (negative number) and the x-axis movement away from drain (usually also negative). The horizontal movement at different distances from the drain pipes is shown as separate plots on each graph. For the graphs depicting vertical movement, the axes are swapped. The individual plots represent different depths. We use the same flow units as we used for the original input, so e.g. pesticide transport is given in g/ha.

B.1 Water

Monthly snapshots of the soil water potential is shown on figure B.1 for all three drain seasons, and the preceding summers. We see shallow groundwater at the beginning of the first drain season, where we overestimate drain flow (see figure C.8). The horizontal movement flux is largest near the drain pipes, and at the bottom of the plow layer in (figure B.2). We also see the largest upward flux below the drain pipes, and downward flux above the drain pipes (figure B.3). Most of the movement within the soil is through biopores (figure B.4).

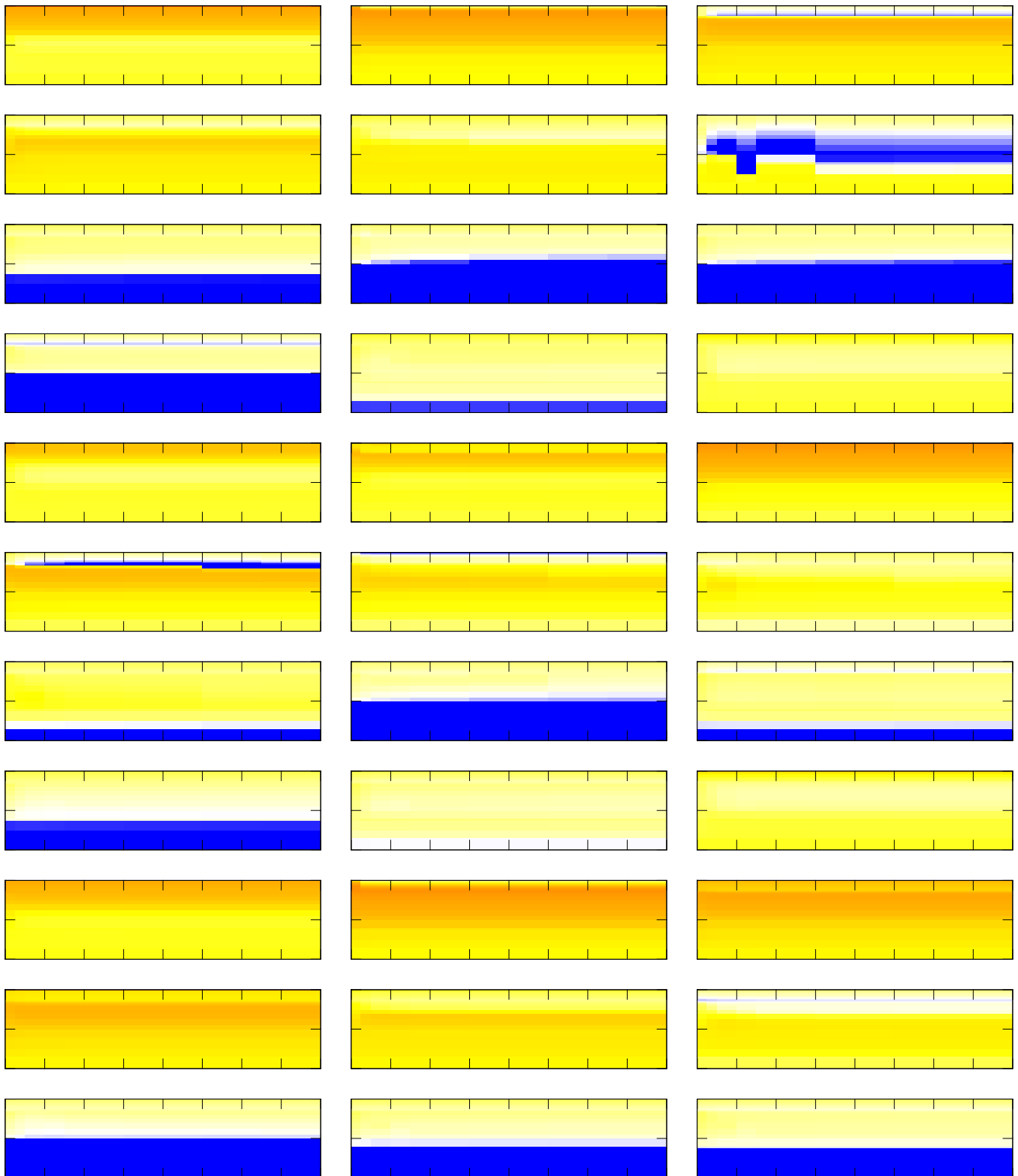


Figure B.1: Soil water pressure potential at the end of each month from May 1998 (top left) to January 2001 (bottom right). The y-axis denotes depth, the x-axis distance from drain. There are tick marks for every meter. Blue denotes $pF < 0$, white $pF = 1$, yellow $pF = 2$, orange $pF = 3$, red $pF = 4$, and black $pF > 5$.

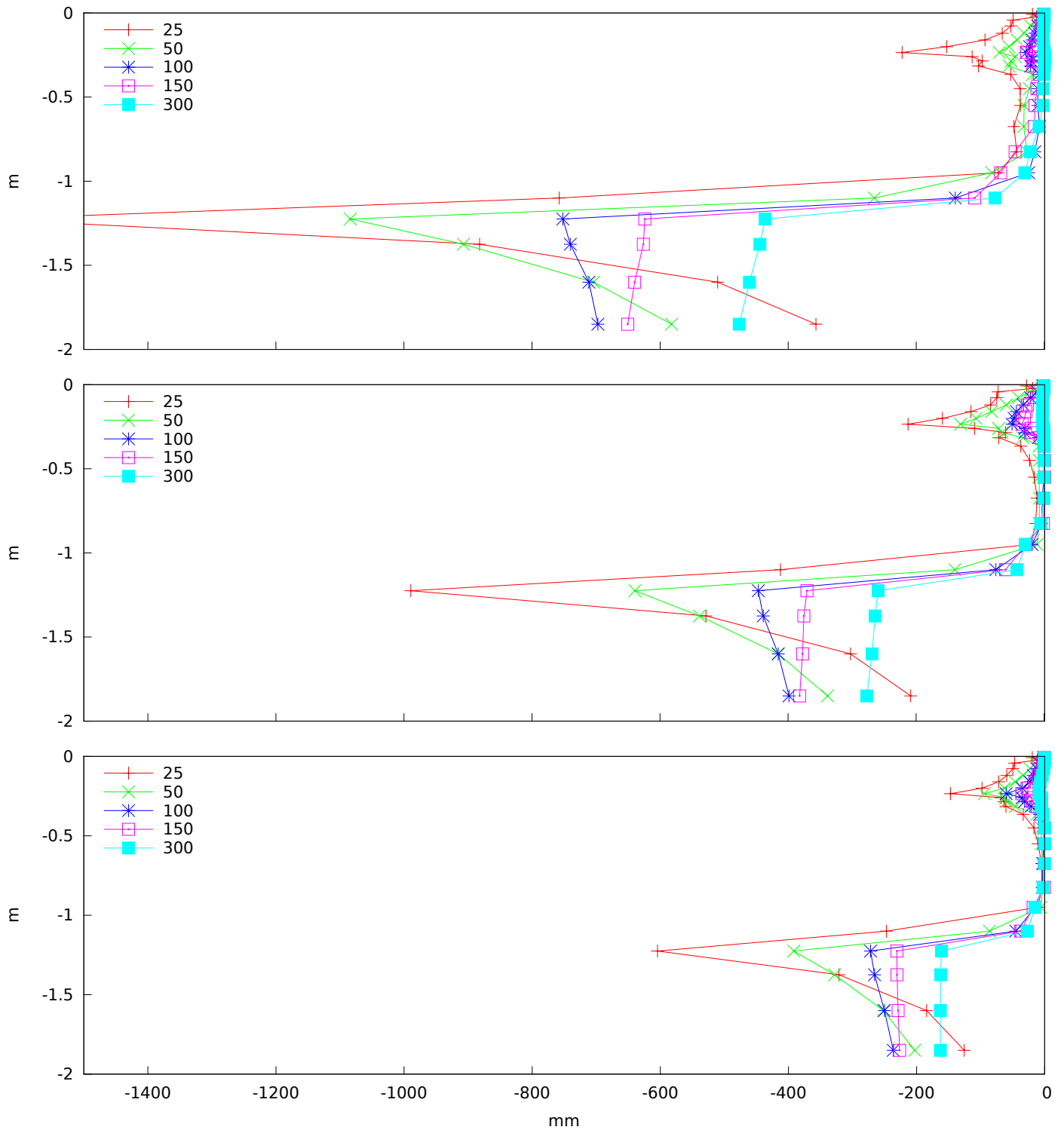


Figure B.2: Horizontal water flux between 1998-5-1 and 1999-5-1 (top), between 1999-5-1 and 2000-5-1 (center), and between 2000-5-1 and 2001-2-1 (bottom). The flux is shown on the x-axis (positive away from drain) as a function of depth shown on the y-axis. The graph labels are the distance from drain in centimeters.

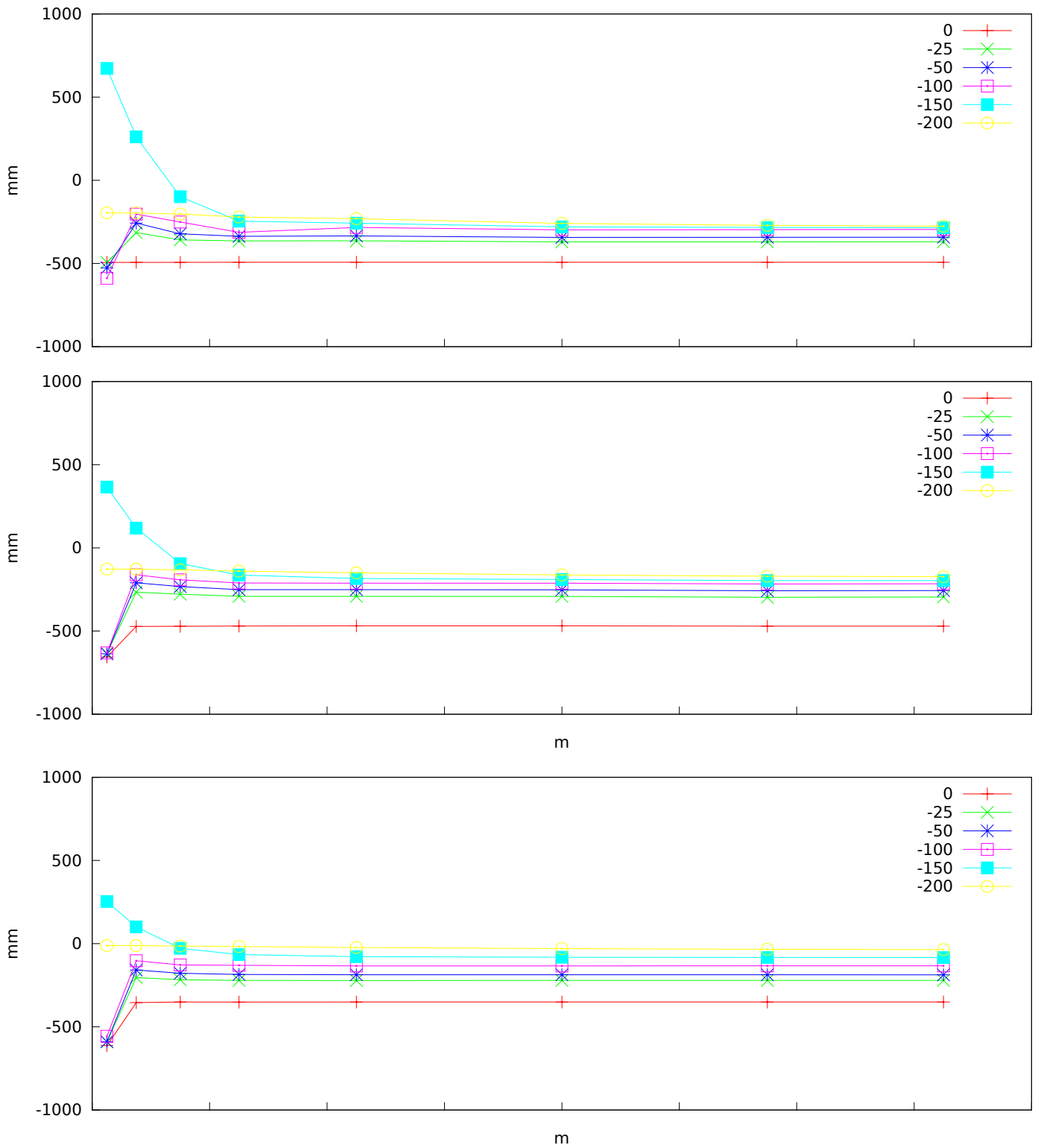


Figure B.3: Total vertical water flux between 1998-5-1 and 1999-5-1 (top), between 1999-5-1 and 2000-5-1 (center), and between 2000-5-1 and 2001-2-1 (bottom). The flux is shown on the y-axis (positive up) as a function of distance from drain shown on the x-axis. The graph labels are depths in centimeters above surface.

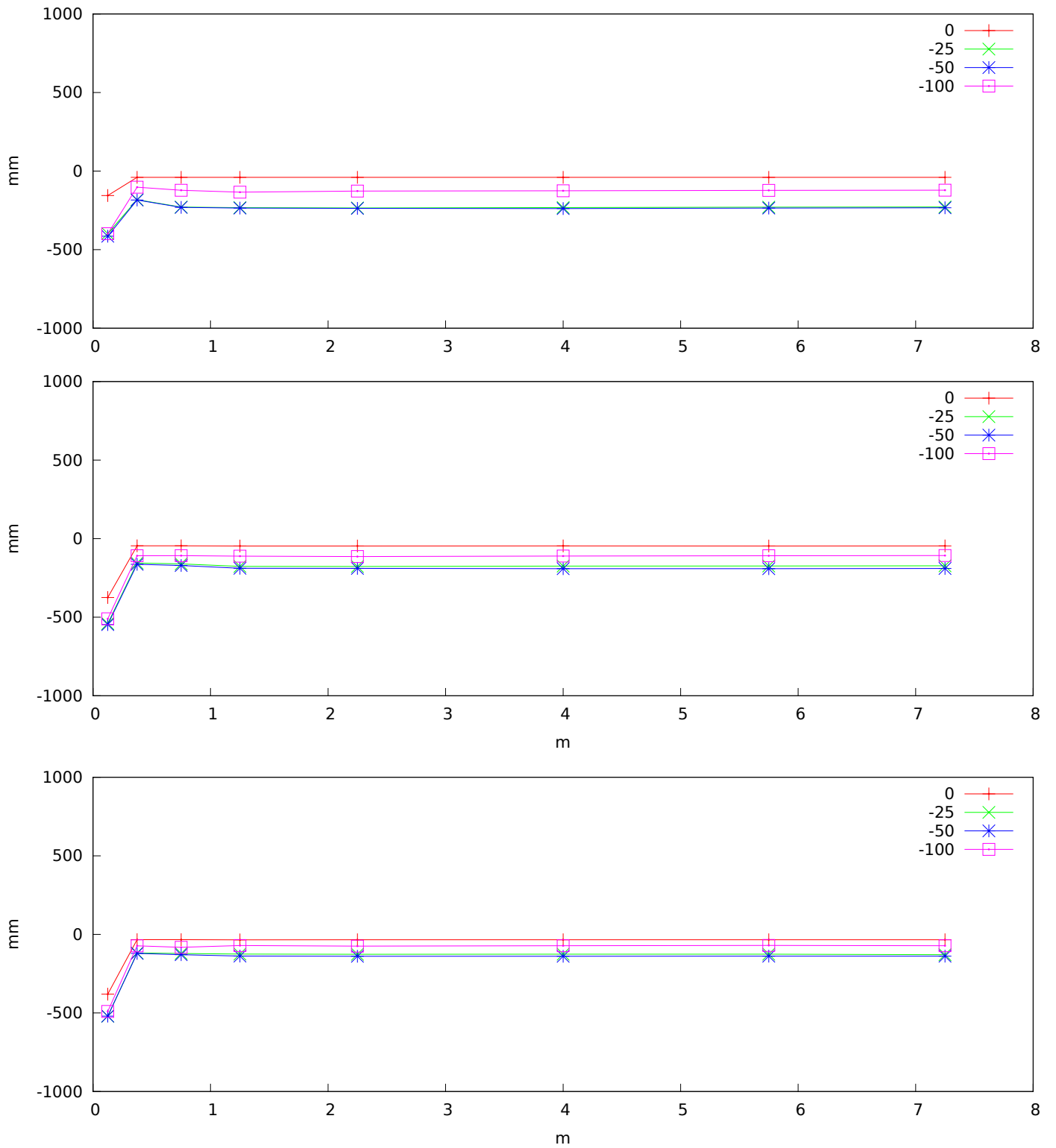


Figure B.4: Biopore water flux between 1998-5-1 and 1999-5-1 (top), between 1999-5-1 and 2000-5-1 (center), and between 2000-5-1 and 2001-2-1 (bottom). The flux is shown on the y-axis (positive up) as a function of distance from drain shown on the x-axis. The graph labels are depths in centimeters above surface.

B.2 Bromide

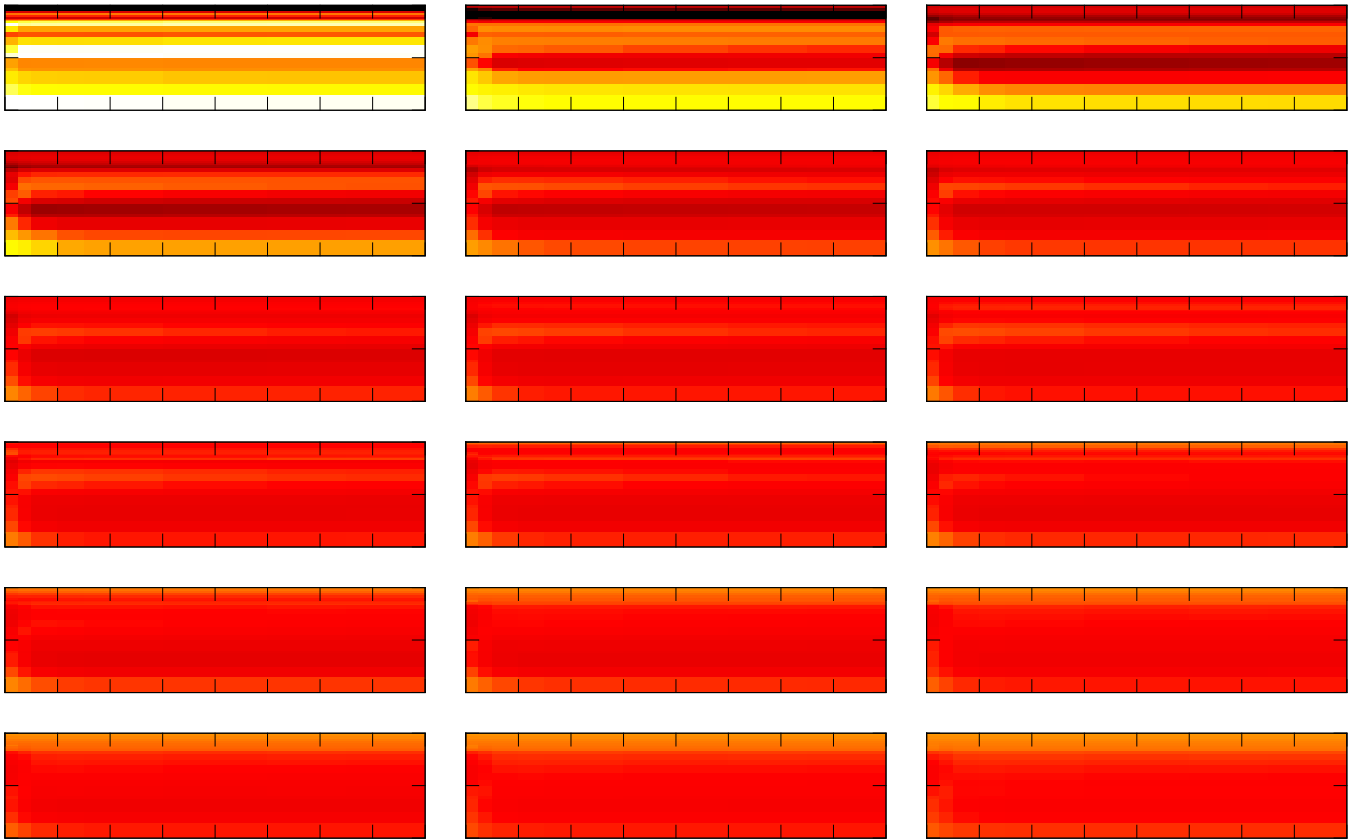


Figure B.5: Bromide soil content at the end of each month since first application in November 1998 (top left graph) until April 2000 (bottom right graph). The y-axis denotes depth, the x-axis distance from drain. There are tick marks for every meter. The color scale is white $< 1 \mu\text{g/l}$, yellow = $10 \mu\text{g/l}$, orange = $100 \mu\text{g/l}$, red = 1 mg/l , and black $> 10 \text{ mg/l}$

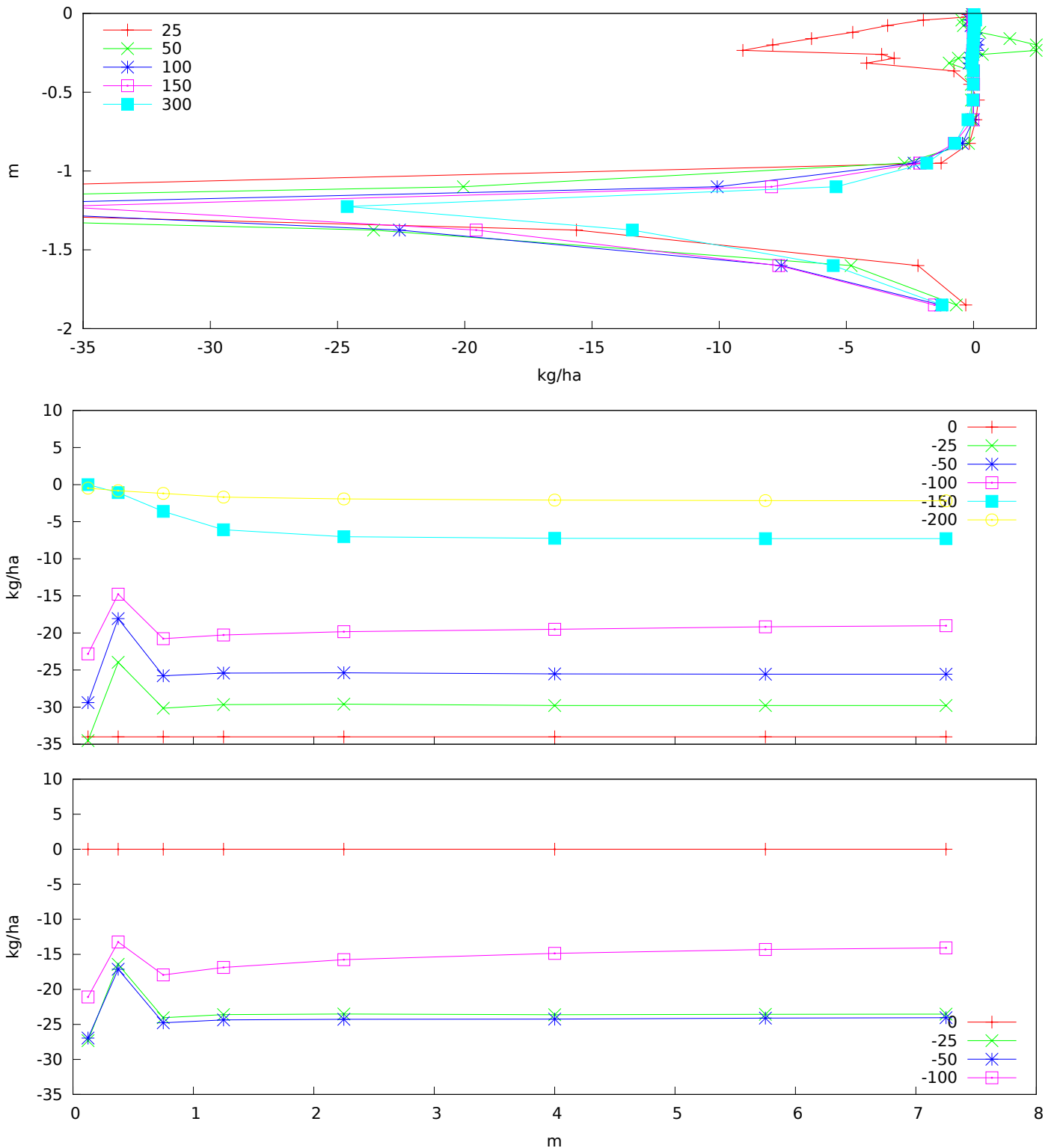


Figure B.6: Bromide transport between 1998-5-1 and 1999-5-1. The top graph show horizontal transport (top), the center graph show total vertical transport, and the bottom graph show biopore transport only. The transport in the top graph is shown on the x-axis (positive away from drain) as a function of depth shown on the y-axis, with graph labels indicating the distance from drain in centimeters. The transport on the two lower graphs are shown on the y-axis (positive up) as a function of distance from drain shown on the x-axis. The graph labels are depths in centimeters above surface.

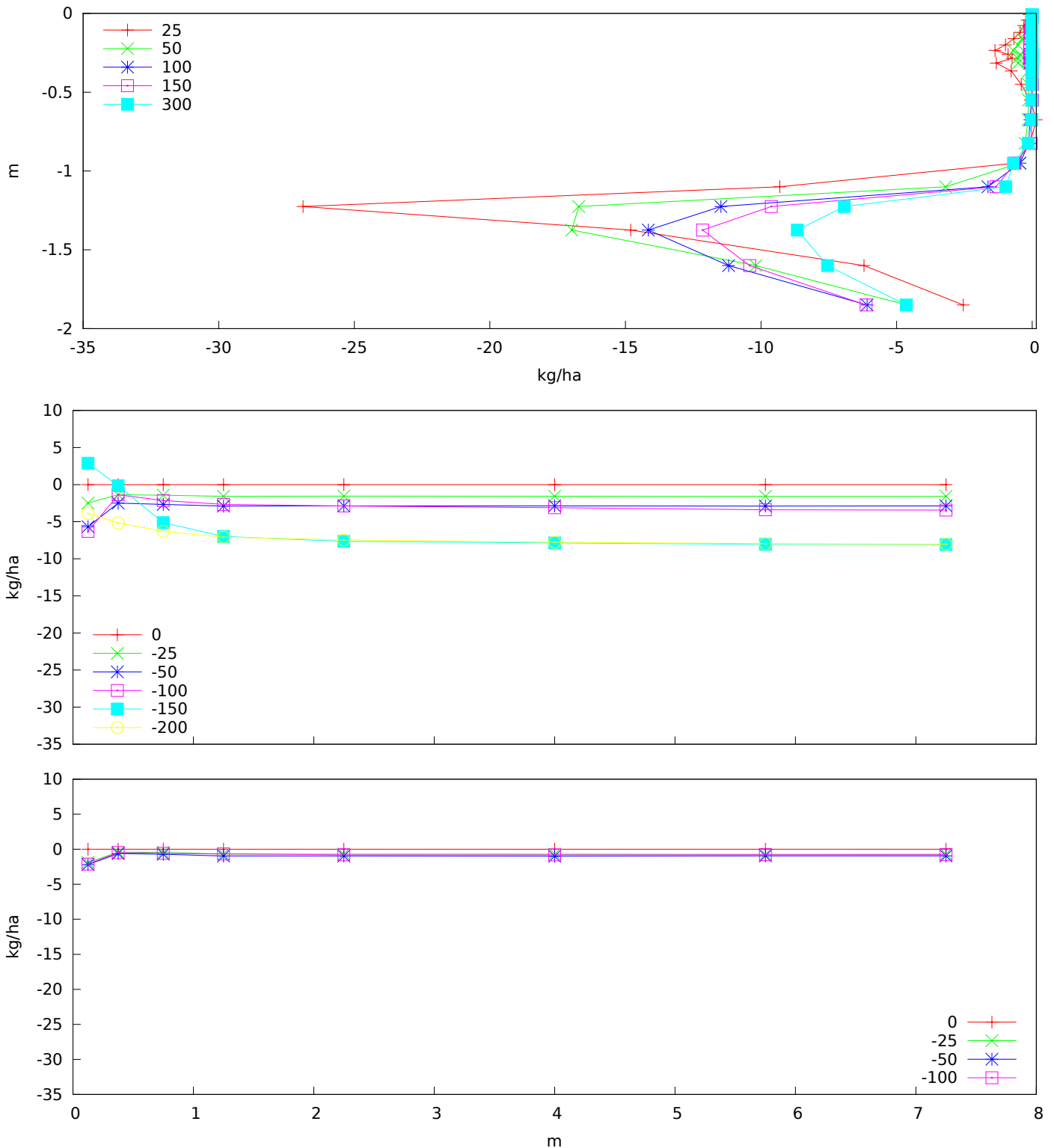


Figure B.7: Bromide transport between 1999-5-1 and 2000-5-1. The top graph show horizontal transport (top), the center graph show total vertical transport, and the bottom graph show biopore transport only. The transport in the top graph is shown on the x-axis (positive away from drain) as a function of depth shown on the y-axis, with graph labels indicating the distance from drain in centimeters. The transport on the two Lowery graphs are shown on the y-axis (positive up) as a function of distance from drain shown on the x-axis. The graph labels are depths in centimeters above surface.

B.3 Pendimethalin

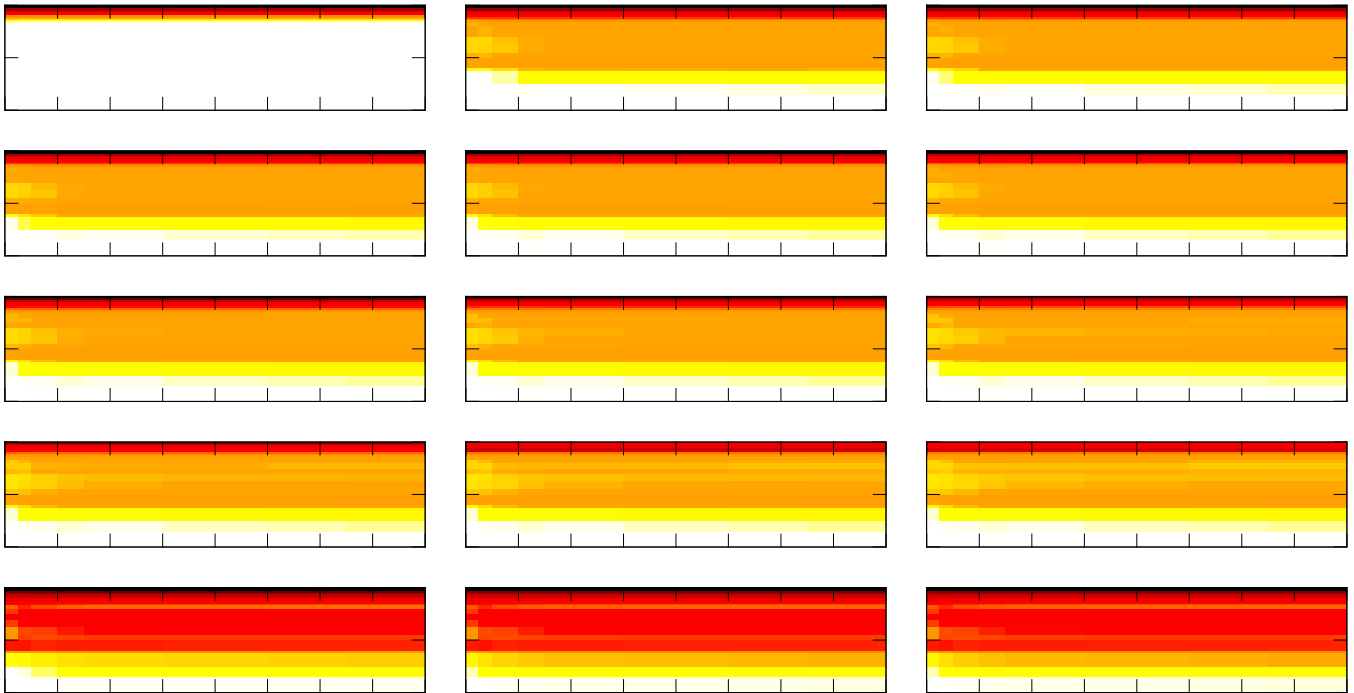


Figure B.8: Pendimethalin soil content at the end of each month since first application in November 1999 (top left graph) until January 2001 (bottom right graph) . The y-axis denotes depth, the x-axis distance from drain. There are tick marks for every meter. The color scale is white < 10 pg/l, yellow = 1 ng/l, orange = $0.1 \mu\text{g/l}$, red = $10 \mu\text{g/l}$, and black $> 1 \text{ mg/l}$

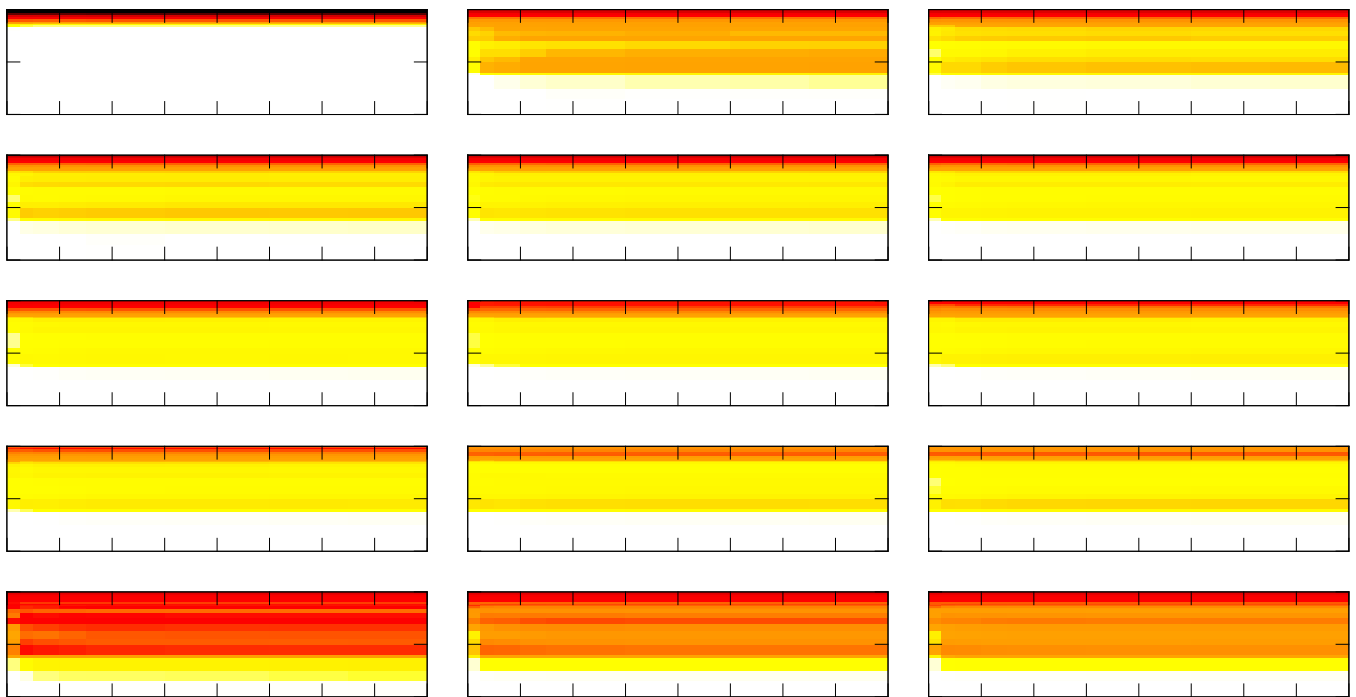


Figure B.9: Pendimethalin soil water content at the end of each month since first application in November 1999 (top left graph) until January 2001 (bottom right graph) . The y-axis denotes depth, the x-axis distance from drain. There are tick marks for every meter. The color scale is white $<10 \text{ pg/l}$, yellow $=1 \text{ ng/l}$, orange $=0.1 \text{ } \mu\text{g/l}$, red $=10 \text{ } \mu\text{g/l}$, and black $>1 \text{ mg/l}$

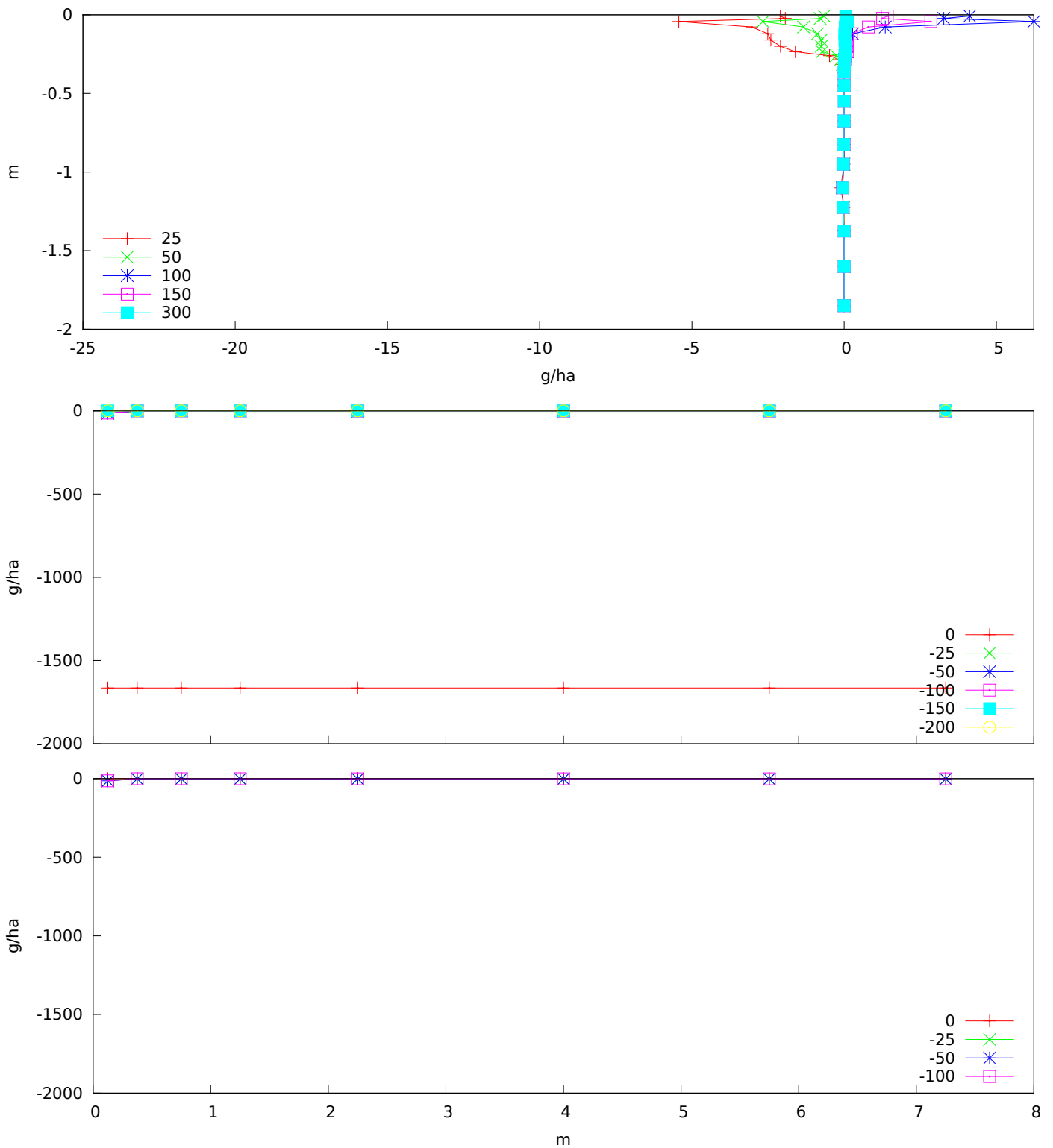


Figure B.10: Pendimethalin transport between 1999-5-1 and 2000-5-1. The top graph show horizontal transport (top), the center graph show total vertical transport, and the bottom graph show biopore transport only. The transport in the top graph is shown on the x-axis (positive away from drain) as a function of depth shown on the y-axis, with graph labels indicating the distance from drain in centimeters. The transport on the two lower graphs are shown on the y-axis (positive up) as a function of distance from drain shown on the x-axis. The graph labels are depths in centimeters above surface.

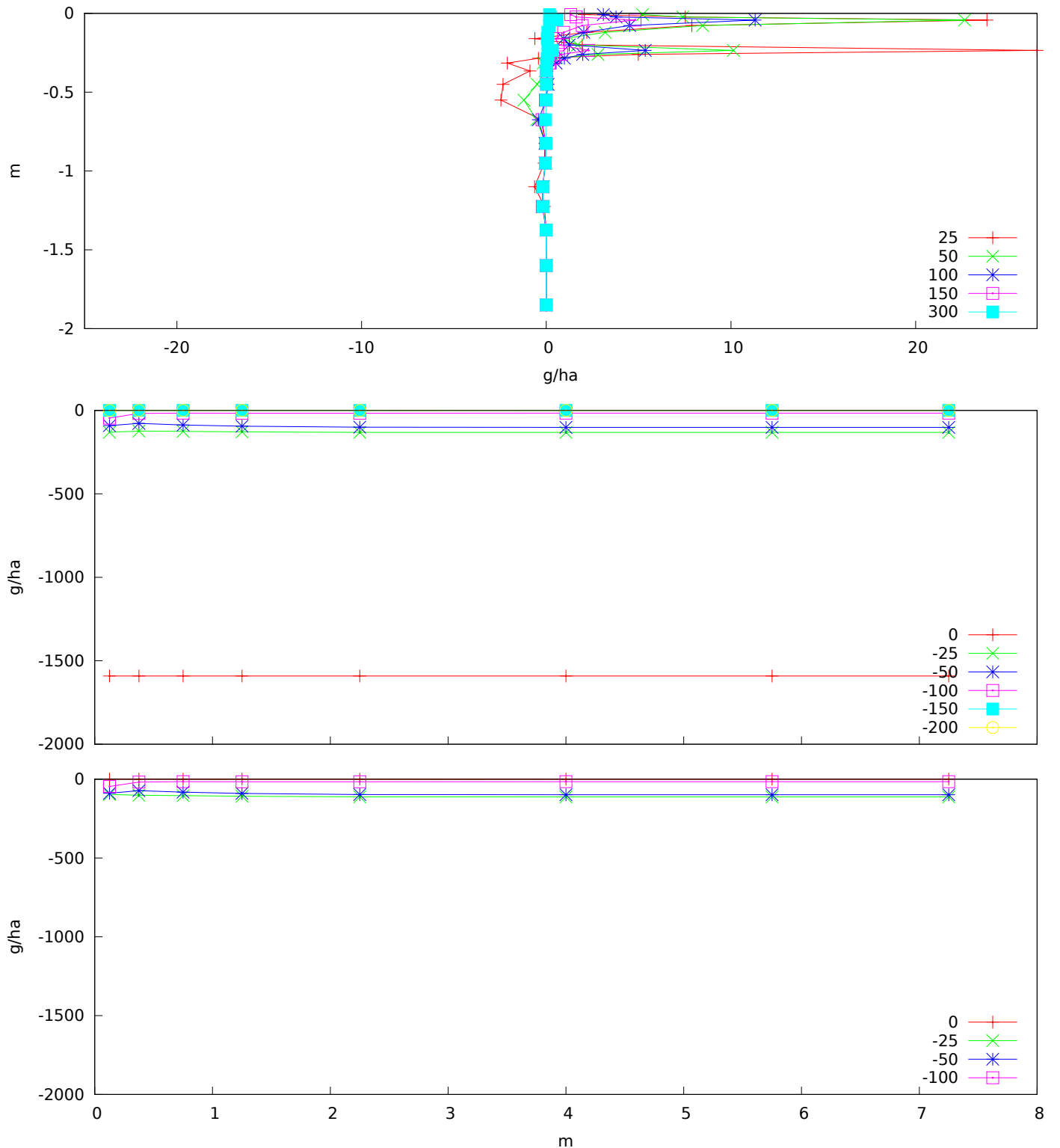


Figure B.11: Pendimethalin transport between 2000-5-1 and 2001-2-1. The top graph show horizontal transport (top), the center graph show total vertical transport, and the bottom graph show biopore transport only. The transport in the top graph is shown on the x-axis (positive away from drain) as a function of depth shown on the y-axis, with graph labels indicating the distance from drain in centimeters. The transport on the two lower graphs are shown on the y-axis (positive up) as a function of distance from drain shown on the x-axis. The graph labels are depths in centimeters above surface.

B.4 Ioxynil

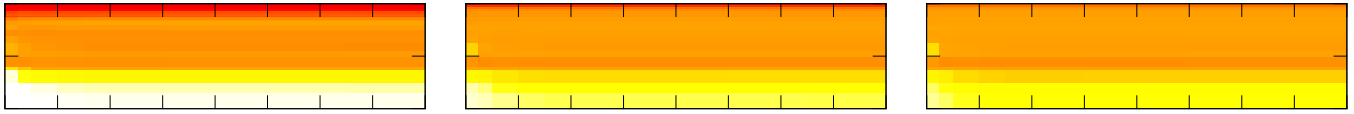


Figure B.12: Ioxynil soil content at the end of each month since first application in November 2000 (top left graph) until January 2001 (bottom right graph) . The y-axis denotes depth, the x-axis distance from drain. There are tick marks for every meter. The color scale is white<math><10\text{ pg/l}</math>, yellow=1 ng/l, orange=0.1 $\mu\text{g/l}$, red=10 $\mu\text{g/l}$, and black>1 mg/l



Figure B.13: Ioxynil soil water content at the end of each month since first application in November 2000 (left graph) until January 2001 (right graph) . The y-axis denotes depth, the x-axis distance from drain. There are tick marks for every meter. The color scale is white<math><10\text{ pg/l}</math>, yellow=1 ng/l, orange=0.1 $\mu\text{g/l}$, red=10 $\mu\text{g/l}$, and black>1 mg/l

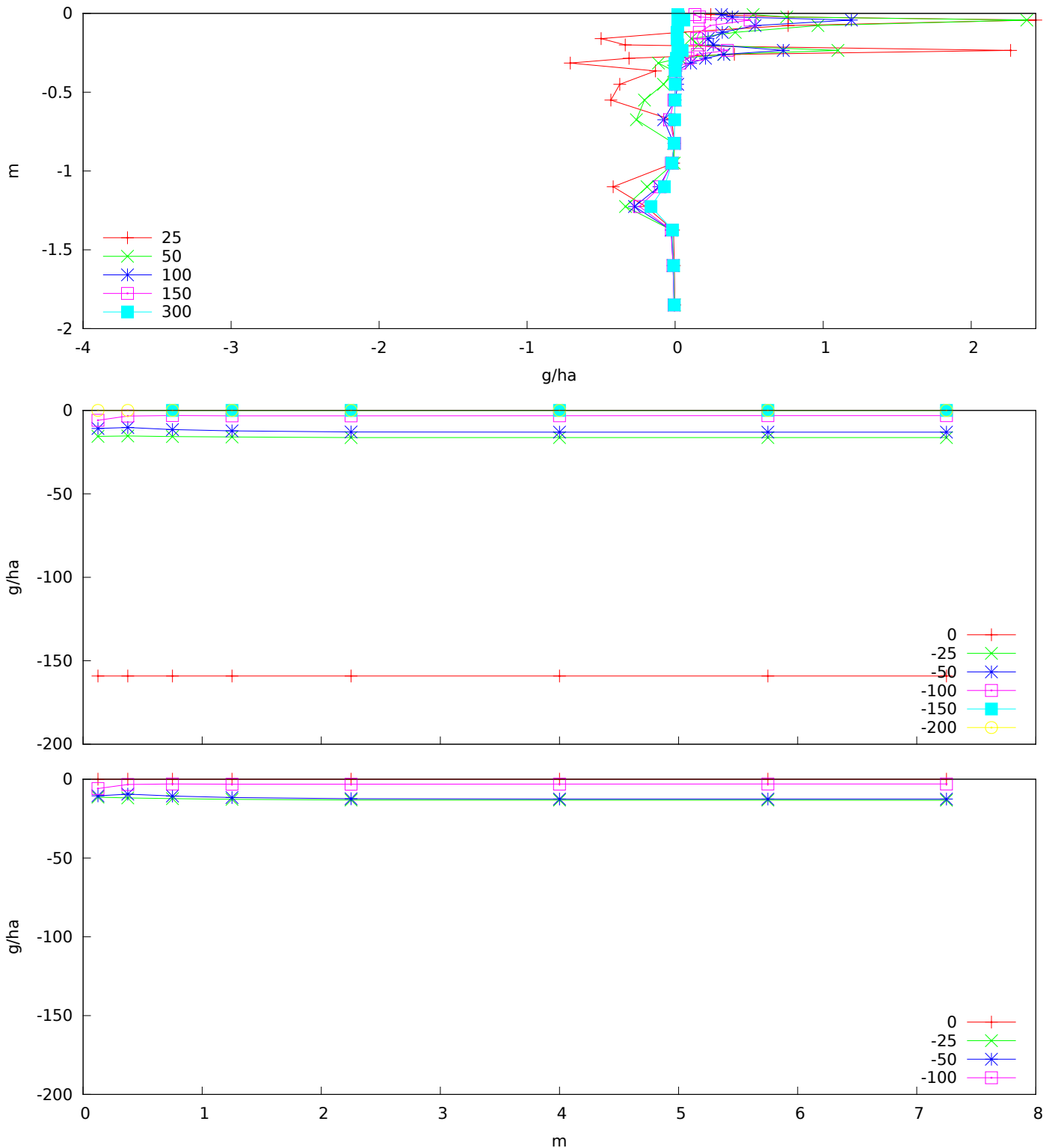


Figure B.14: Ioxynil transport between 2000-11-1 and 2001-2-1. The top graph show horizontal transport (top), the center graph show total vertical transport, and the bottom graph show biopore transport only. The transport in the top graph is shown on the x-axis (positive away from drain) as a function of depth shown on the y-axis, with graph labels indicating the distance from drain in centimeters. The transport on the two lower graphs are shown on the y-axis (positive up) as a function of distance from drain shown on the x-axis. The graph labels are depths in centimeters above surface.

Appendix C

Time series

The comparison between measured and simulated numbers are presented in this appendix. The figures have a high information density, and have therefore been allowed to fill most of the page. Each figure contains multiple graphs, all of which share the same x-axis. This structure is intended to facilitate comparison. The same figures were used for calibration. All figures show precipitation (left axis) and air temperature (right axis) for the period in the top graph.

All drain measurements were done with flow proportional sampling, with variable timestep. For comparison with the hourly simulated results, samples representing less than one hour of flow very combined.

C.1 Soil water content

The graphs on figure C.1 and C.3 shows simulated and measured volumetric water content at different depths, and are discussed in section 3.1.

C.2 Soil bromide content

Figures C.4, C.5, C.6, and C.7 concern soil bromide content, and are discussed in section 3.2.

C.3 Drain content

The full drain seasons are depicted on figure C.8, C.10, and C.12, while figure C.9, C.11, and C.13 focus on a single event within each drain season. See section 3.3.

Dynamic and accumulated water flow is shown on the two first graphs under the top graph. The median piezometer pressure table, and the calibrated aquifer pressure is shown on the right axis on the dynamic water flow graph. See section 3.3.1. The next two graphs show particle leaching. The dynamic particle leaching represent particles collected since last measurement. The particles may have leached before the time of measurements. The simulated reservoir of ready available particles is shown on the same graph. See section 3.3.2

The next graphs depend on season. For season 1998–1999 and season 1999–2000 (figures C.8 – C.11) the next two graphs depicts bromide concentration, and accumulated bromide leaching. For season 2000–2001 they instead depict ioxynil concentration and mass in drain water. For the 1999–2000 and 2000–2001 season, we finish off with pendimethalin concentration and mass. For the pesticides, we both colloid bound and total amounts are shown. See section 3.3.3.

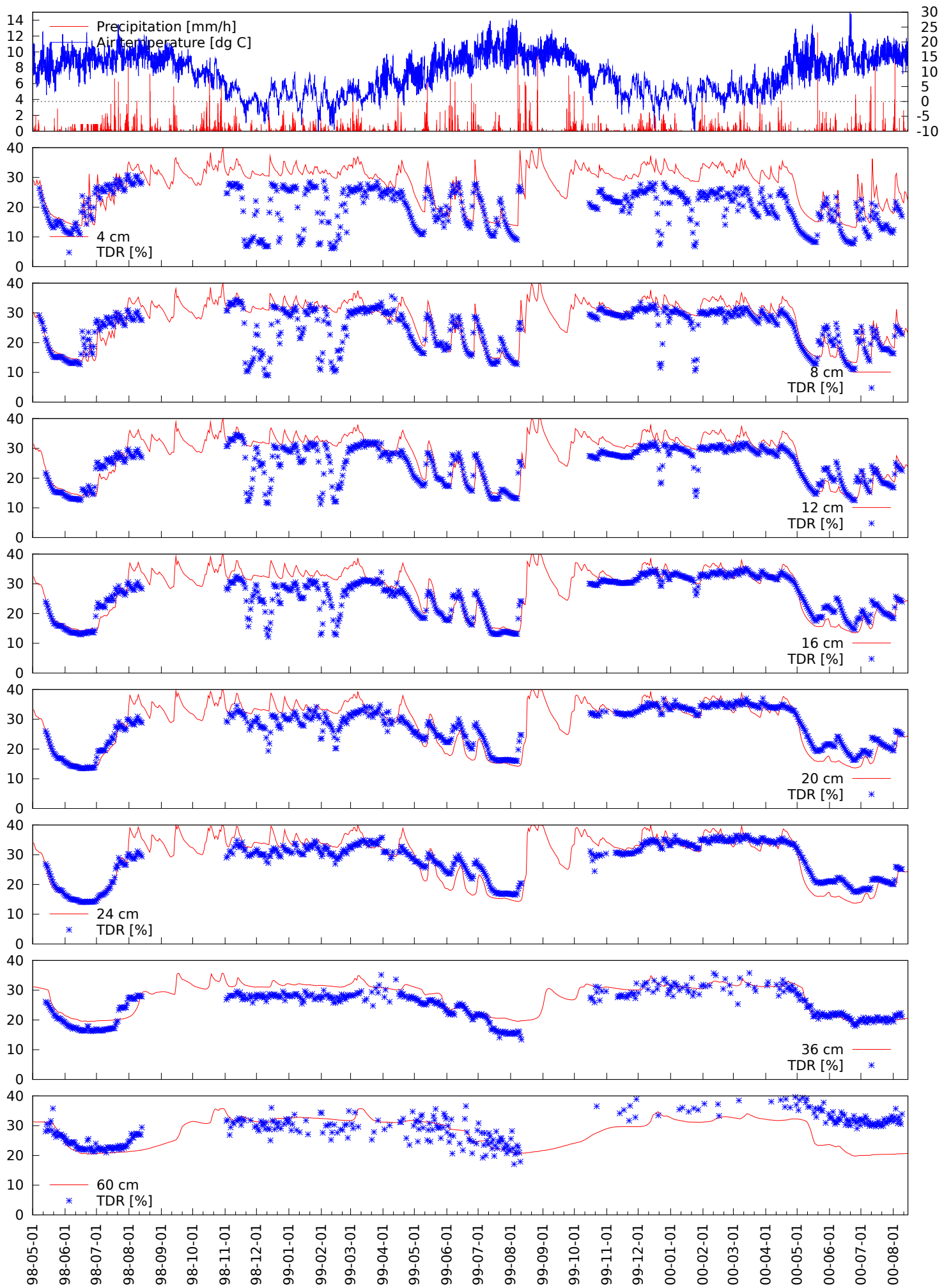


Figure C.1: TDR measurements.

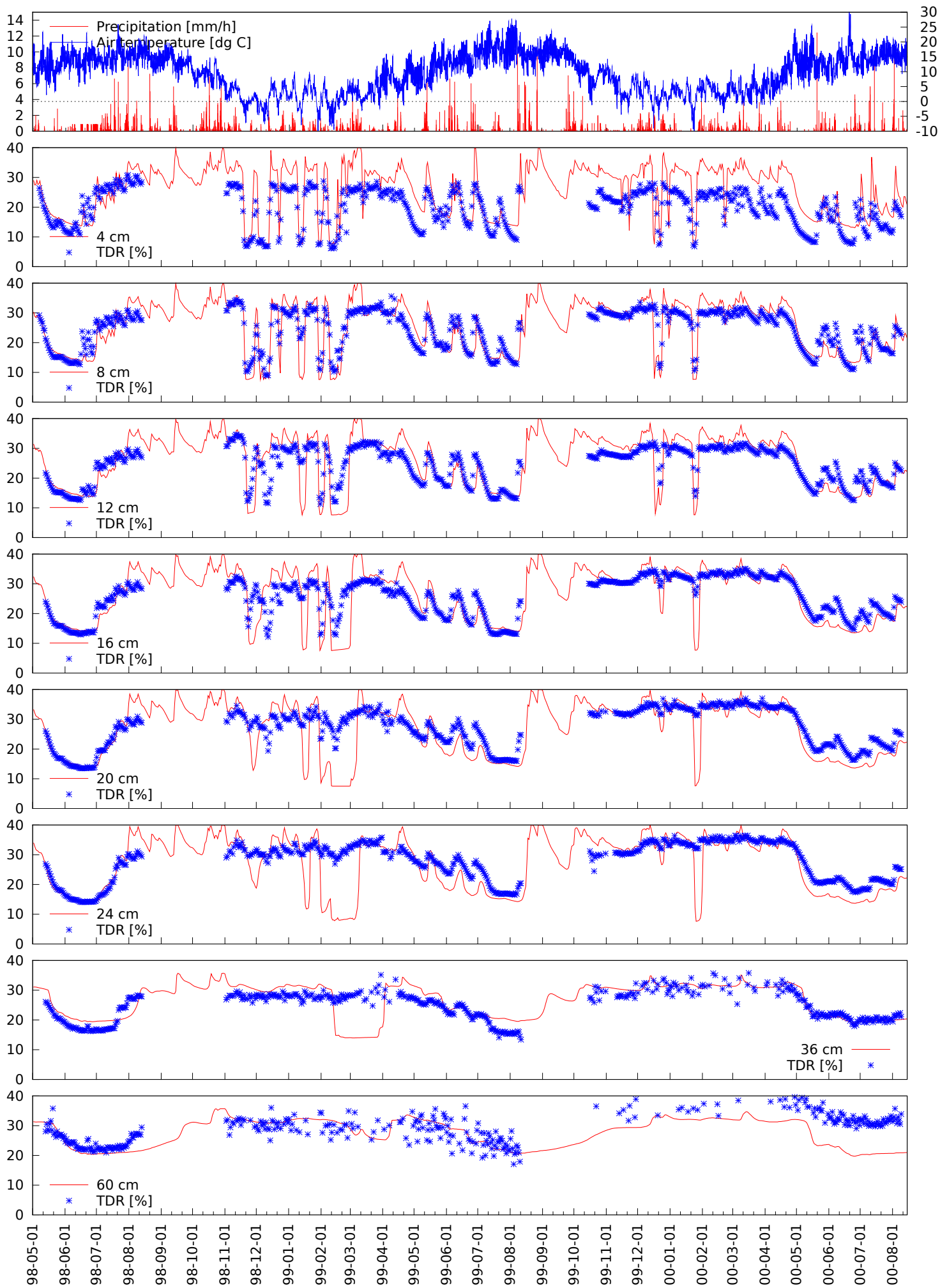


Figure C.2: TDR measurements compared to experimental run with ice enabled.

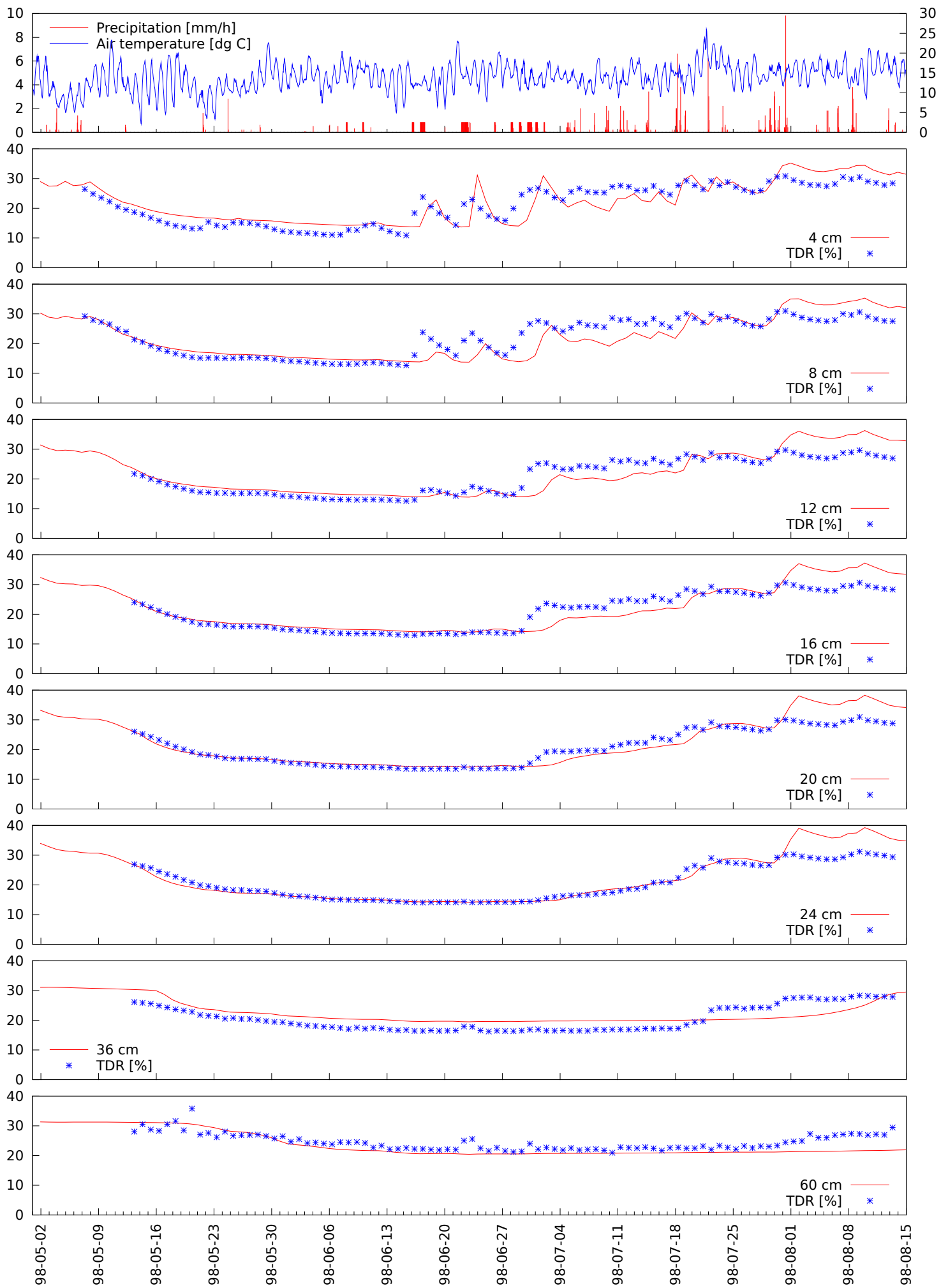


Figure C.3: Early TDR measurements.

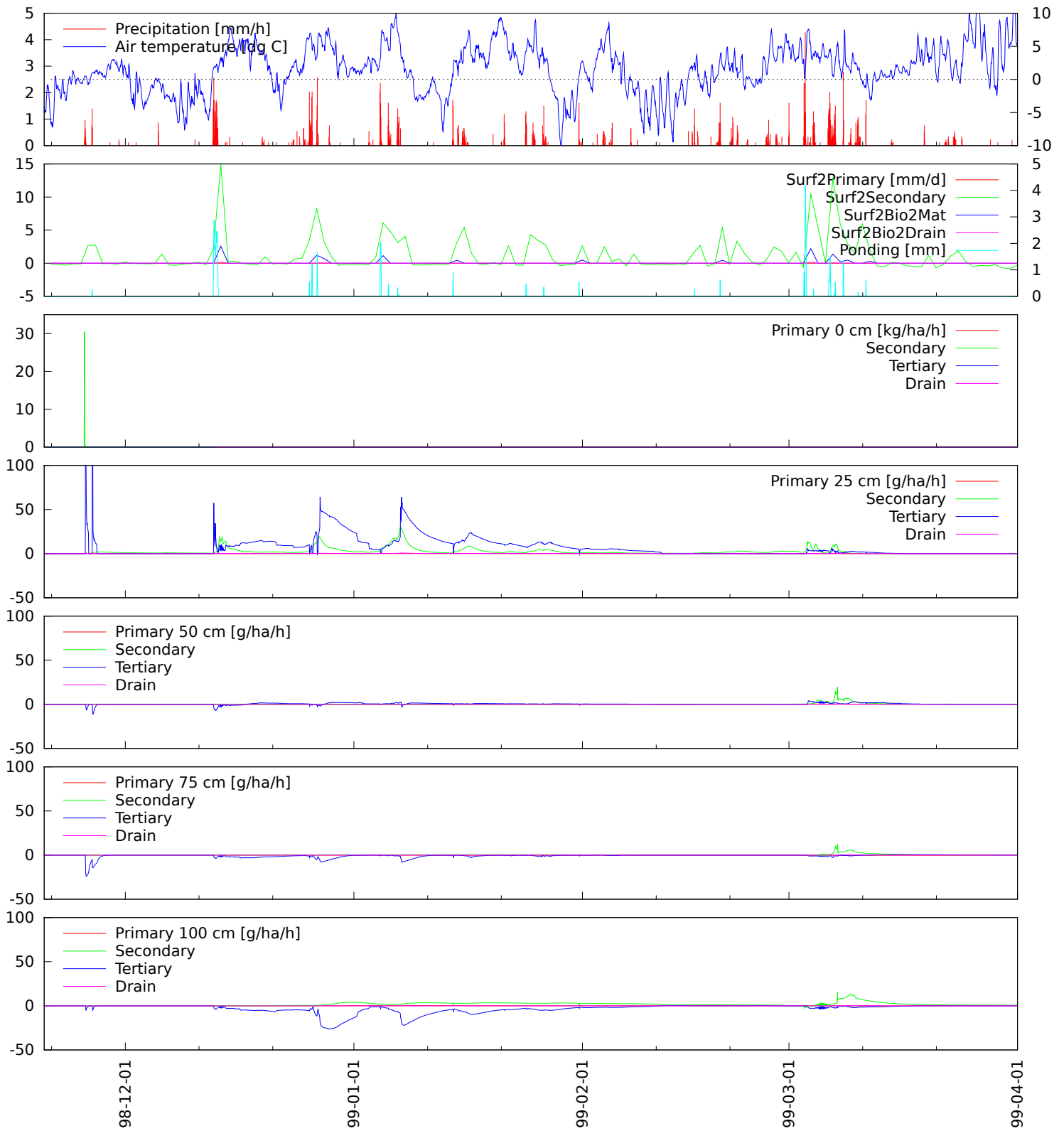


Figure C.4: Bromide dynamics.

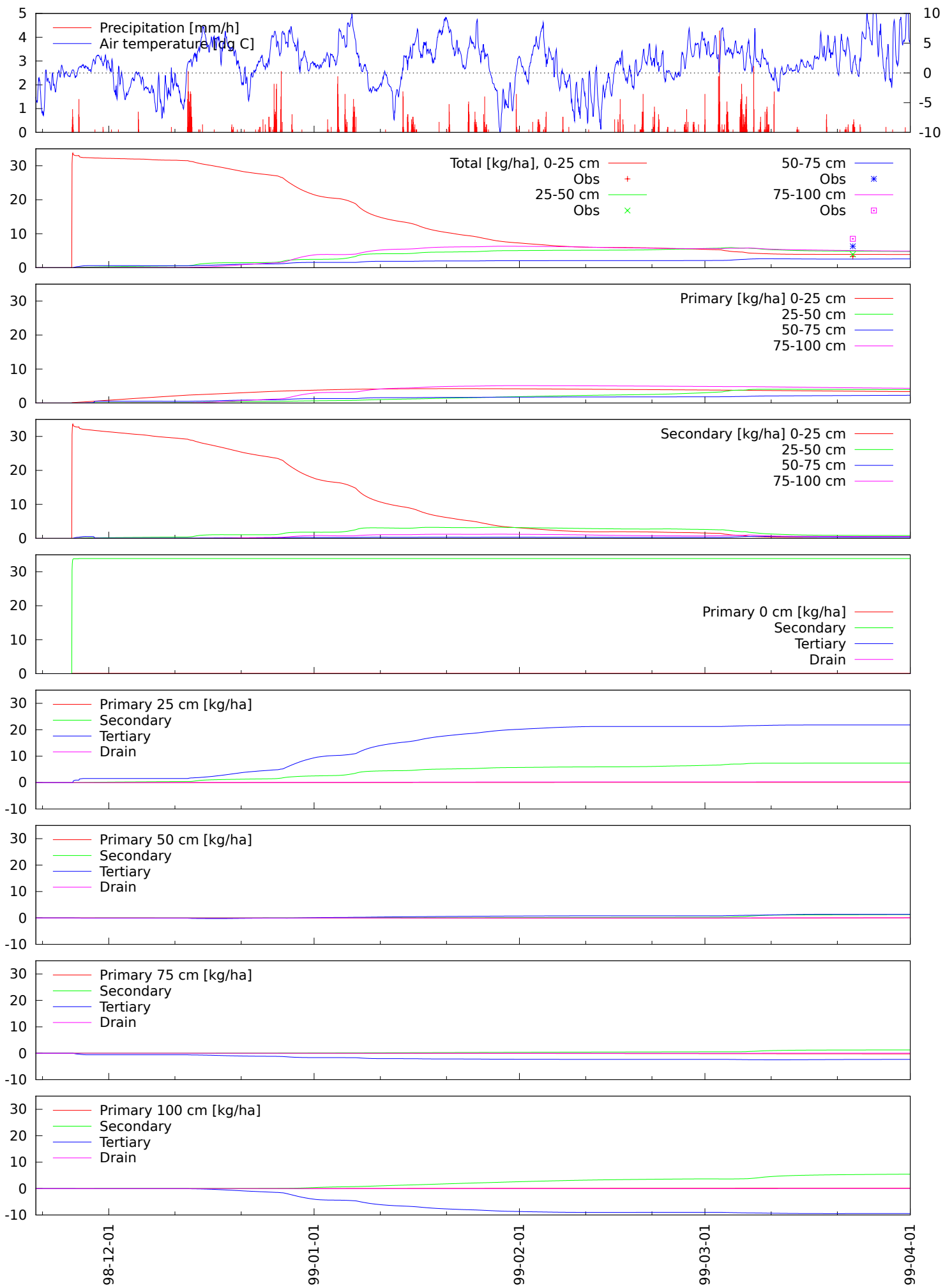


Figure C.5: Accumulated bromide.

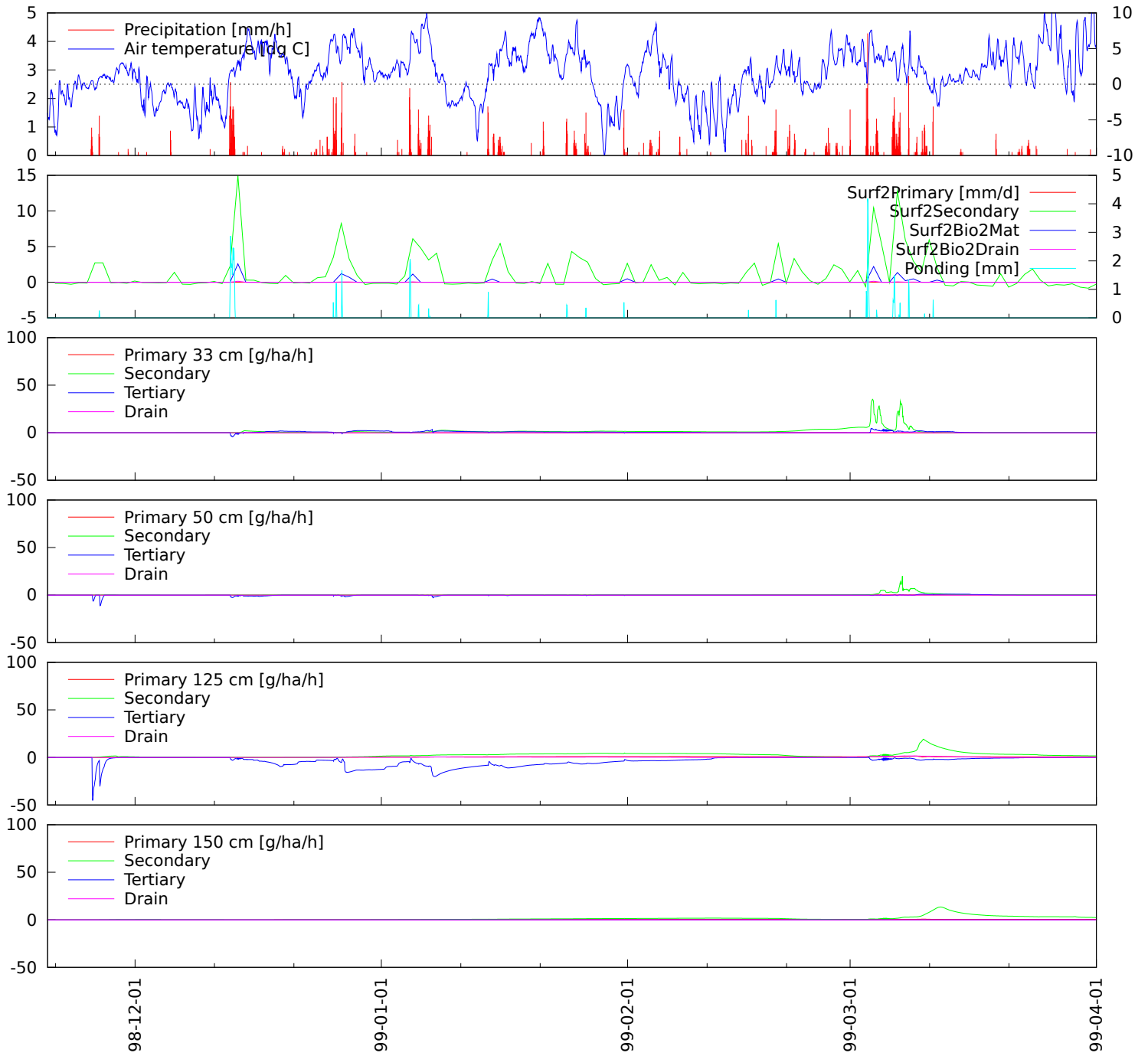


Figure C.6: Bromide dynamics (extra).

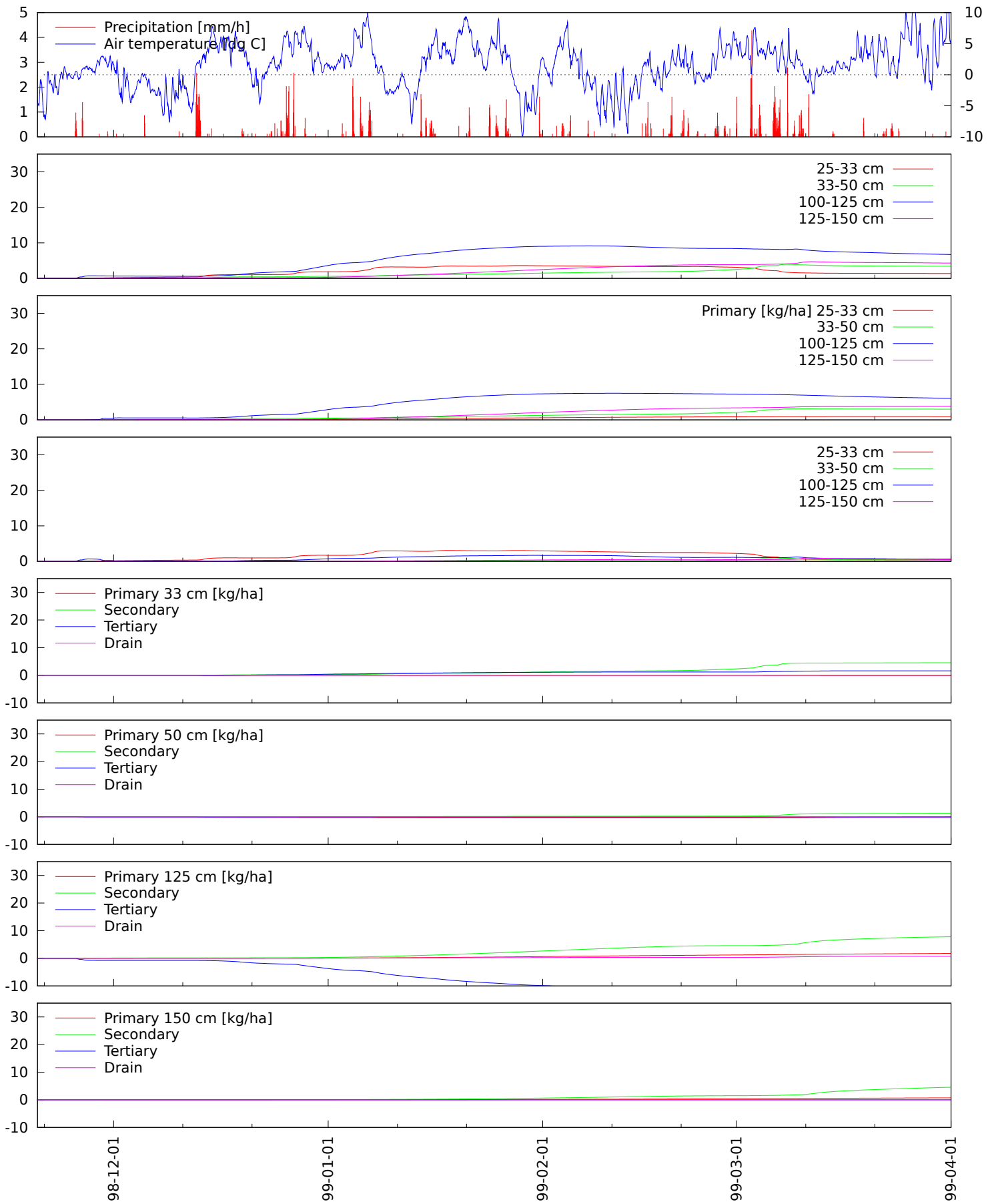


Figure C.7: Accumulated bromide (extra).

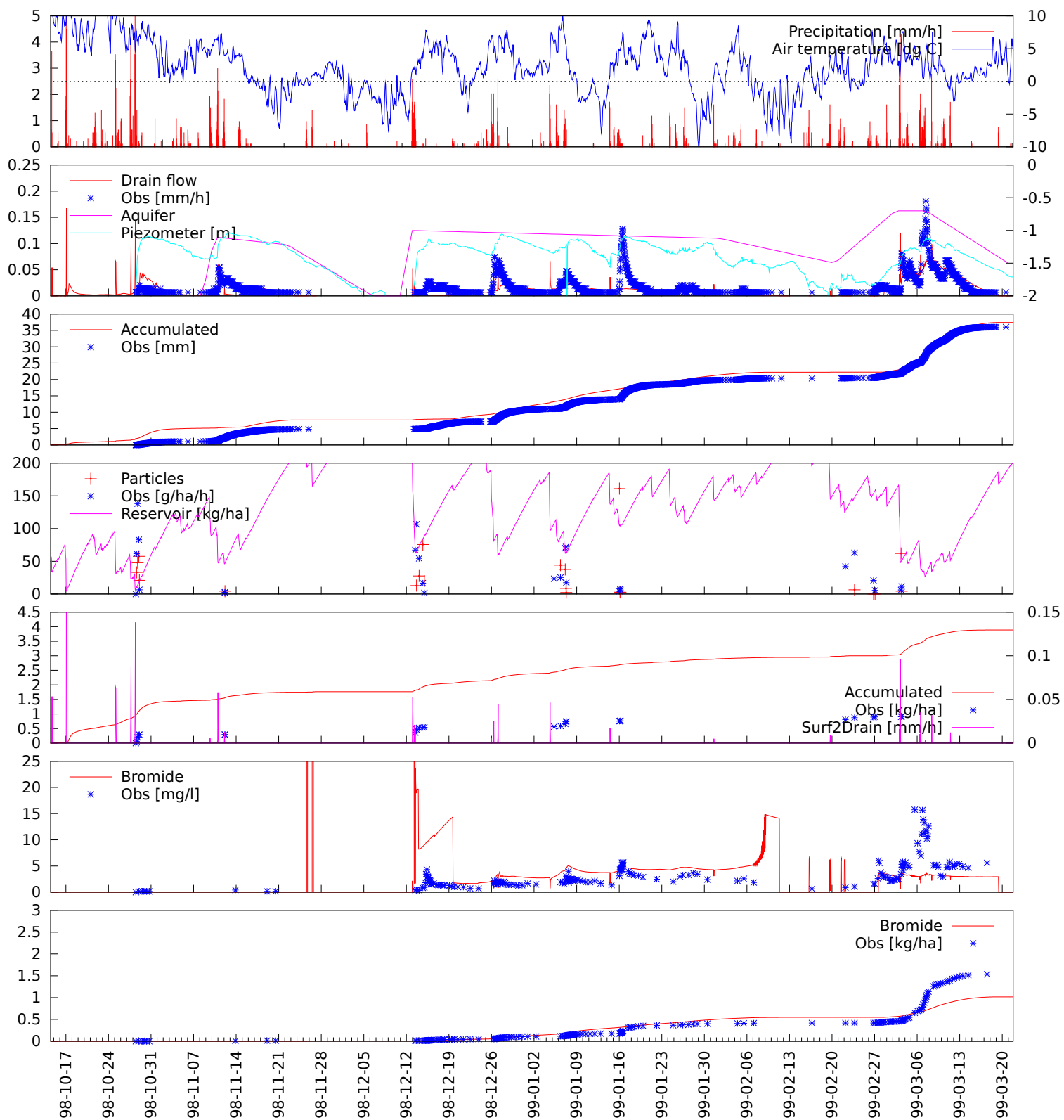


Figure C.8: Drain season 1998 – 1999.

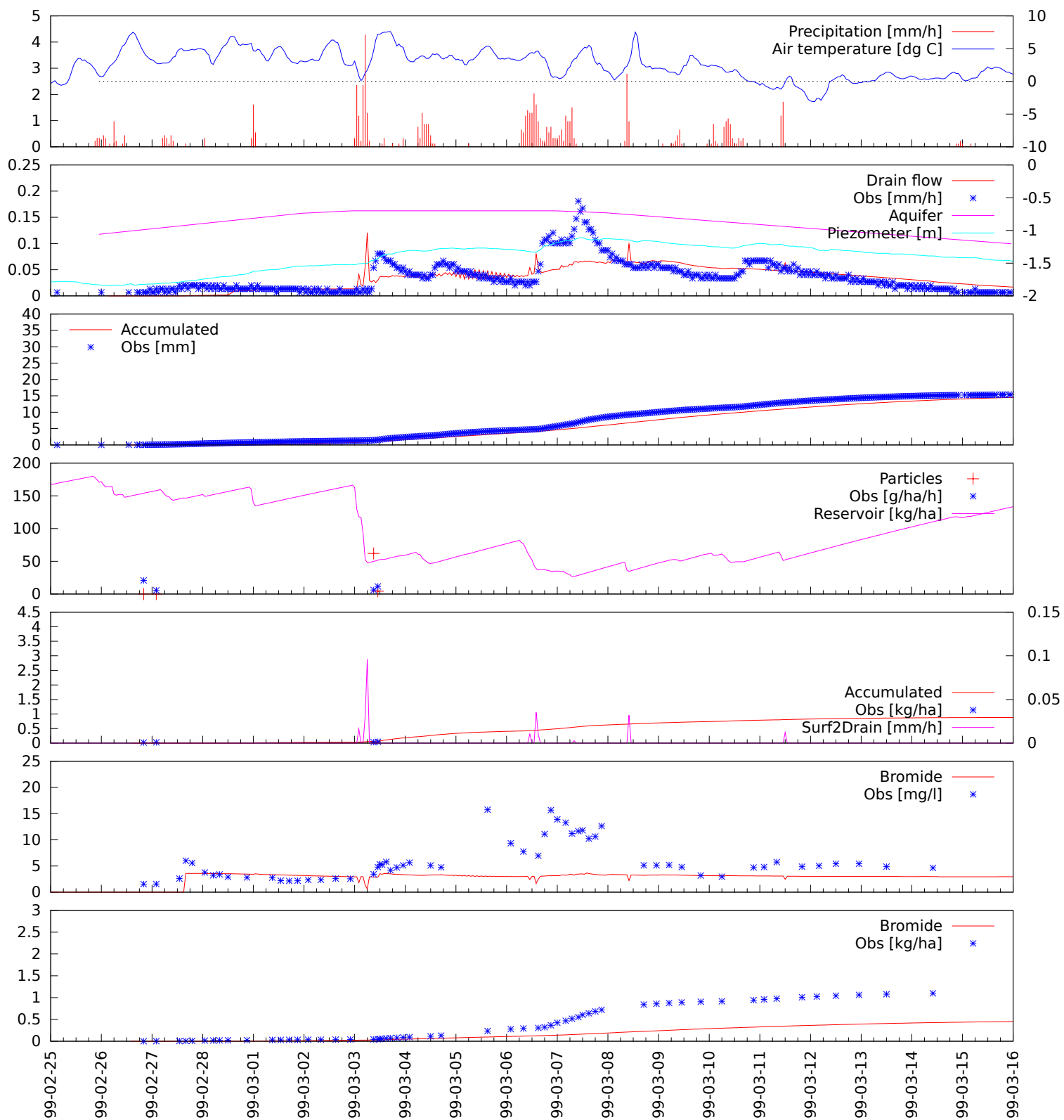


Figure C.9: Drain season 1998 — 1999, single event.

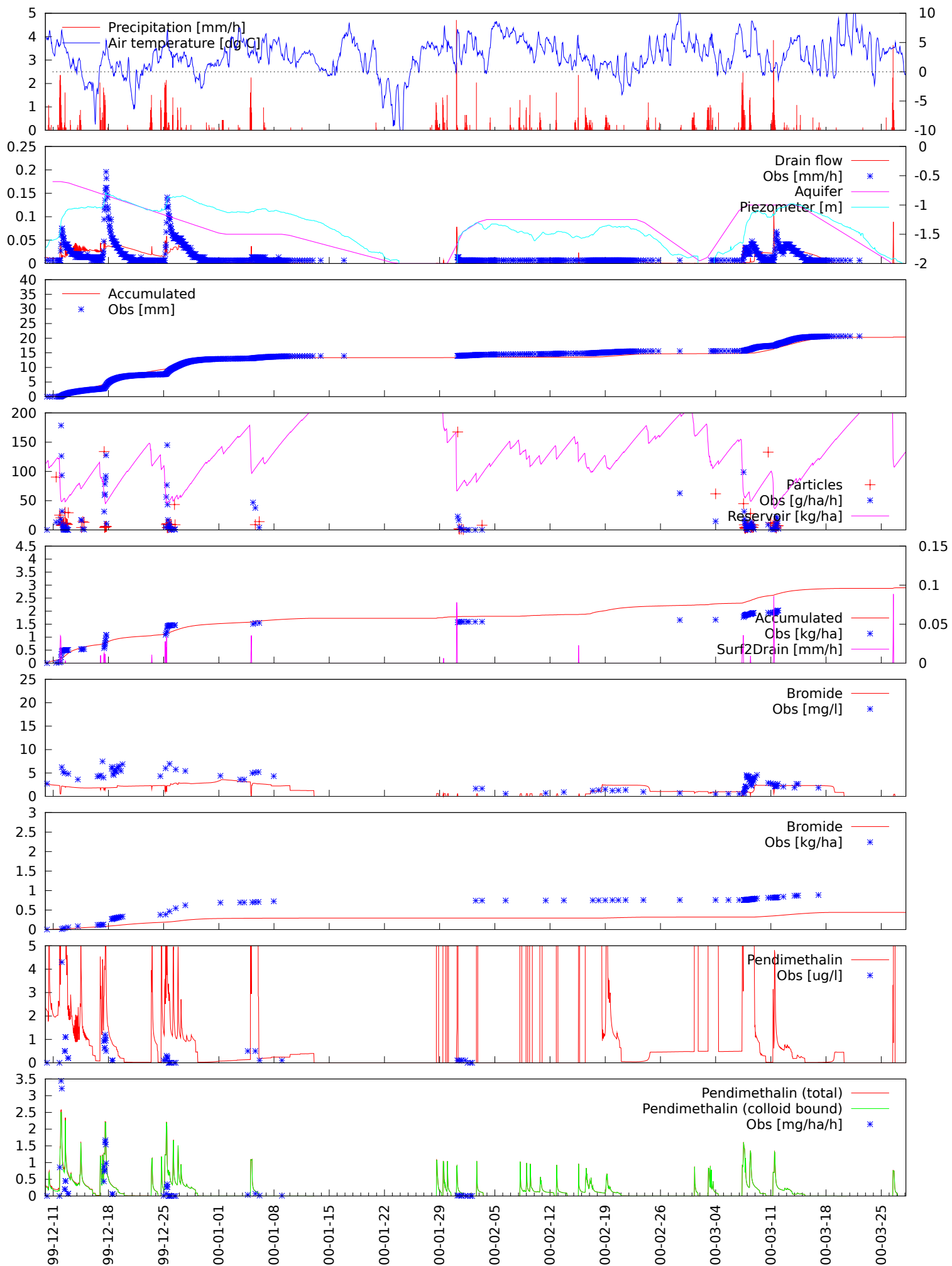


Figure C.10: Drain season 1999 — 2000.

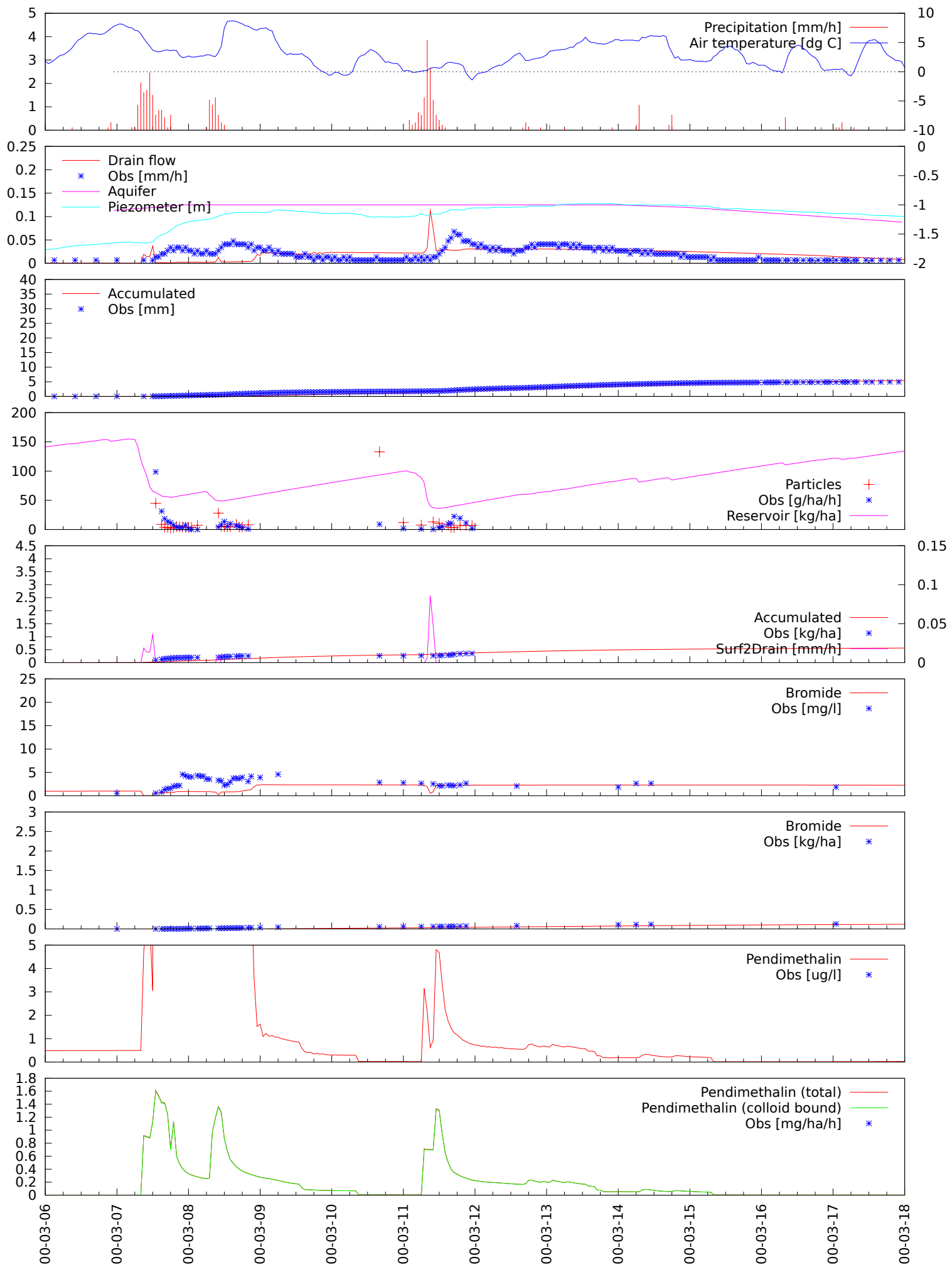


Figure C.11: Drain season 1999 — 2000, single event.

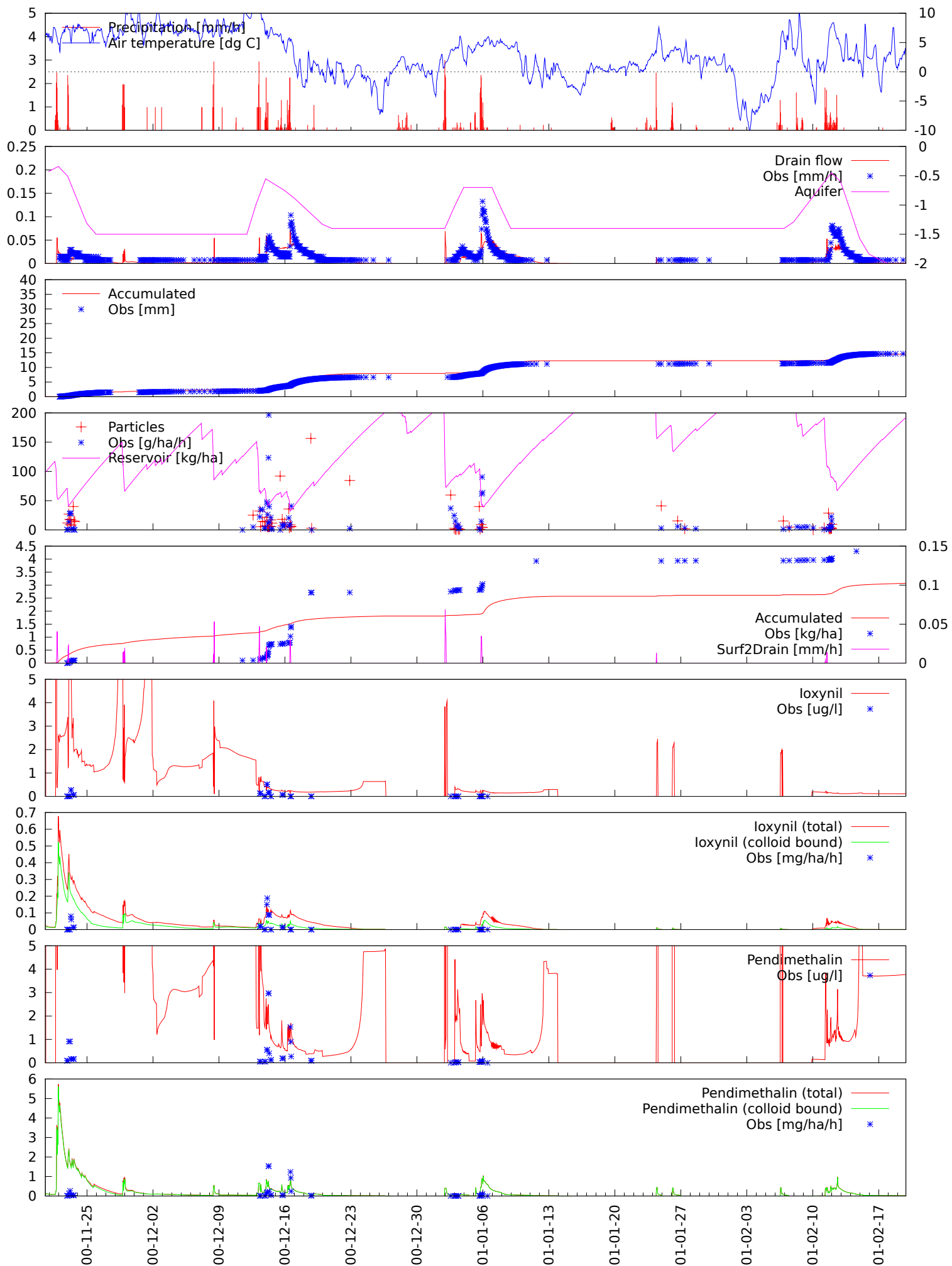


Figure C.12: Drain season 2000 — 2001.

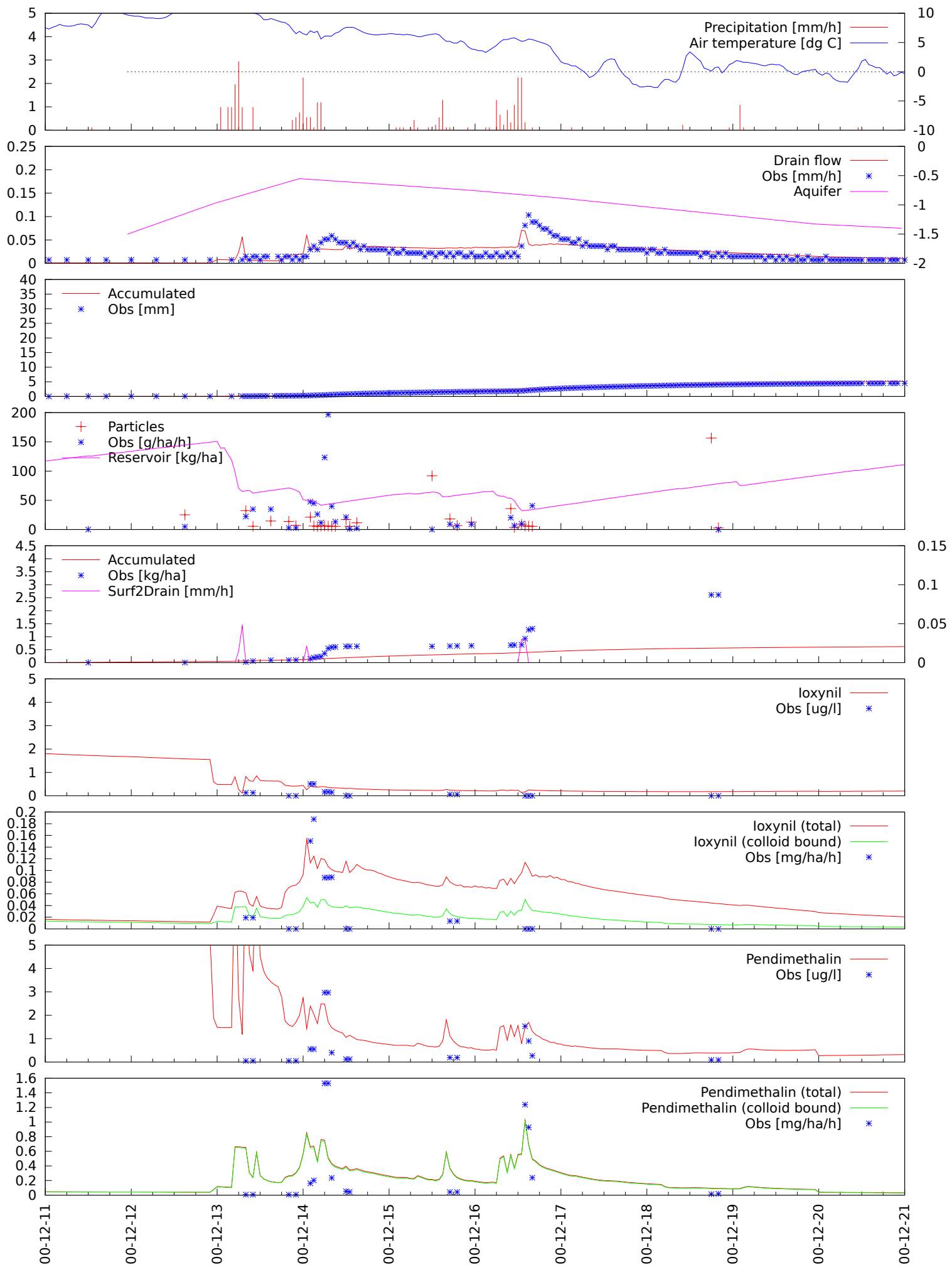


Figure C.13: Drain season 2000 — 2001, single event.